STUDY OF PHOTONIC CRYSTAL BASED WAVEGUIDE AND CHANNEL DROP FILTER AND LOCALIZATION OF LIGHT IN PHOTONIC CRYSTAL

Wei Jiang

Institute for Fusion Studies and Department of Physics, University of Texas, Austin, TX 78712

(May 15, 2000)

Master's Thesis

SUPERVISOR: Herbert L. Berk

Abstract

The major part of thesis addressed theoretical problems arising in Photonic Crystal based novel devices, like waveguides and channel drop filters. A perturbation theory based on band theory is proposed for 2-dimensional (2-D) waveguides and is verified in 1-D waveguides. This theory shows excellent agreement with the exact theory in 1-D case for enough large band gap. This theory also predicts that the propagating constant of the modes may not be zero at the lower edge of the band gap, no matter for 1-D or 2-D case. This is verified by the exact theory in 1-D case. In 2-D case, where an exact theory is not possible, it is opposed to the numerical results of another group of researchers but supported by experimental data. We proposed a full group theory approach to channel drop filters. In light of this theory, we show the difficulty lying generate high order flat-top can be easily overcome by enhancing the symmetry of the system, instead of simply increasing the number of cavities. As an example, we calculate the 3-fold symmetry case. We find that the localization of light in Photonic Crystal undergoes a trilogy by simulation. This unexpected phenomenon is analyzed by introducing a novel measure for localization problems: the C number. Finally, we understand the trilogy is due to the competition of two localization mechanisms with different ranges of coherence. We show a localization picture where Anderson model is insufficient to explain.

I. INTRODUCTION

A. Overview: History and Perspective

During the second half of this century, the development of semiconductor technology has brought about enormous changes to our society and the life of people. The trend for even higher density of integration and faster processors pushes the miniaturization to the extreme for electronic devices. The high resistance and therefore long delay time associated with the small feature size, and the synchronization problem arising from high speed transmission of data becomes more and more serious for electronic devices[1].

At this turn of the century, there is a possibility that photonic devices may take over the role that electronic devices now have in our life. Nothing propagates faster than light. Due to the high frequency nature of the light, the available bandwidth of photonic devices is also much higher than conventional electronic devices can provide. Photons are Bosons, hence they are not restricted by the Pauli exclusion principle. Therefore, arbitrarily high density of photon field can be achieved. This means that the energy density of light can be much higher than in an electron systems. A stereotype example is Lasers. Electrons in solids are frequently scattered by phonons, impurities, which results in high loss at room temperature. Another far-reaching effect of the scattering is that as the energy of the electrons changes, so does their de Broglie wavelength, this makes it impossible to build coherent electronic devices. In photonic devices, the loss of power can be reduced to minimum by proper choice of the medium. While the light lose a small fraction of its power during traveling, for most medium, the inelastic scattering of light is negligibly small. Therefore, the coherence of light is maintained all through its propagation. The coherence of light is essential to its role in the information age.

Photonic Crystals fully employ the coherent nature of the light, and open a new area of promise for the development of all optical integrated circuits. The idea of Photonic Crystals can be traced back to early works done by John, who studied the anomalous absorption

of light in a disordered medium[2], where he noticed the role of localization in anomalous absorption. His continuing work on this problem led him to realize that the presence of a band gap in the spectrum of the photons may result in strong localization even when the disorder is only moderate. Then Yablonovitch proposed and fabricated the first photonic crystal[3], or Photonic Band Gap(PBG) material. The key property of photonic crystals is that the size of unit cells of the crystal is comparable to the wavelength of the light. When light travels in the crystal, the Bragg reflected waves interfere with the original beam. The coherence completely changed the homogeneous distribution of the light field in the crystal, and the dispersion relation of the propagating waves. In another view, the situation is nearly the same as an eletron travelling in a solid, the electron energy spectrum is changed by the scattering of the periodic lattice. However, due to the presence of impurity, defects, thermal motion of the atoms, and many body effects in the solid, the electron spectrum found from purely periodic ionic lattice is not exact. And these complications renders the determination of the true spectrum a very difficult problem. In photonic crystal, the scattering of light is purely electromagnetic, and is governed by the Maxwell equations, which is linear if no nonlinear constitutive relation of the materials is involved. Therefore, the problem can be solved exactly. This enables people to design materials with high accuracy. In Photonic Crystal, the problems of thermal scattering, and many body effects are virtully not present. The thermal effect is restricted to the thermal expansion of the materials which is largely controllable and only results is small shift of the operating wavelength(about a few $nm's$ for the temperature deviation under the typical operating environment of typical electronic devices).

The PBG materials show potential of changing the whole scenario of light guiding in the near future. In the traditional waveguides operated at optical range, the light is guided by the total internal reflection at the boundary of the waveguide. This is quite different from the waveguide operated at microwave range, where the metallic waveguides are used. Though in some sense, the propagation of microwave in such waveguides can also be regarded as internal reflection, but there is no restriction on the reflection angle. For the waveguiding

at optical frequencies, the metallic waveguides result in great loss, the dielectric waveguides are the natural choice. But the reflection is restricted to small incident angle with respect to the waveguide surface. The discovery of photonic crystals put a new "twist" on light guiding. When the frequency of the light falls in the gap of the photonic crystal, it is not able to propagate in the crystal. When such light is incindent on the surface of the crystal, it will be completely reflected for any incident angle. This provides a great deal of flexibility for the guiding of light. A prominent example is to guide the light through a sharp bend with very high efficiency.[4] For photonic waveguides, extensive numerical calculations and experimental study have been conducted by several groups.[1, 5] However, analytical study lags behind. The complexity of the field patterns in the crystal render the analytical treatment a difficult task compared to the analysis of the traditional dielectric waveguide. [6] In the thesis, an analytic theory based on perturbation techniques is proposed and found to agree well with the results of numerical calculations when the frequency is not far from the lower edge of the band gap. This theory is first proposed for the 2-D square lattice. The dispersion relation for a waveguide sandwiched between two 1-D photonic crystal can be solved analytically. The comparison of result of our perturbation theory with the exact dispersion in 1-D system shows excellent agreement near the lower edge of the pseudogap, when the pseudogap is large enough. This shows that the theory has basically captured the essence of theory of the dispersion relation for such waveguides. The key point is matching the logarithmic derivative of the electric (or magnetic) field at the boundary between guided region and the walls of the waveguide. The derivative is generally finite for a frequency at the bandedge and has a linear dependence on the imaginary wavevector(or decay constant) near the lower edge in the gap.

B. Applications of Photonic Crystals

The idea of photonic crystal is exciting, but the realization is not easy. A rule of thumb is that the lattice constant of the photonic crystal is about one half to one third of the

wavelength. Even the wavelength we choose is at the infrared range, say 1.5 μm, this means a lattice constant about 0.5 to 0.8 μm. And the features inside the cell should be even smaller in dimension, about 0.2 to 0.4μm. This is nearly the technological limit of current best microlithography techniques. The electron beam lithography and X-ray lithography are two candidates for improved fabrication of such small features.

However, the versatile cabilities of photonic crystals have become a strong driving force for the continuing study in this area. High quality factor Q cavity is one of the promising applications. [1] This kind of high Q cavity is desirable in laser generation. The free-photon density of states per unit volume is proportional to

$$\frac{1}{\omega\lambda^3} \tag{1.1}$$

In photonic crystal, if the frequency falls in the photonic band gap, the density of state is zero. By introducing a localzed states with frequency in the gap, the density of states near the frequency of the localized state is completely changed. The density of states per unit volume for the resonant frequency scales as

$$\frac{1}{\Delta\omega\Omega} \tag{1.2}$$

where $\Delta\omega$ is the frequency width of the resonance and Ω is its effective spatial volume. The enhancement factor is then given roughly by

$$\frac{\omega}{\Delta\omega}\frac{\lambda^3}{\Omega} = \frac{Q}{\Omega/\lambda^3} \tag{1.3}$$

where $Q \equiv \frac{\omega}{\Delta\omega}$ is the quality factor of the cavity. Thus high Q and small spatial volumes can lead to significant enhancement of spontaneous emission. As the smallest volume Ω must be of the order of λ^3, the largest enhancement available is about Q. To achieve such high enhancement factors, it is essential to fabricate cavities with spatial dimensions comparable to the wavelength of light. Photonic crystals with single defect is one of the simplest way to realize such microcavities, though the fabrication requires state-of-the-art lithographic techniques. But calculations show that the quality of the microcavities are

not quite sensitive to the surface disorder which will definitely be present due to the small feature size. This insenitiveness gives the hope to fabricate a microcavity of practical use.

A novel application of the photonic crystal is related to the channel drop filters which is an important component of wavelength division multiplexing(WDM) devices. Due to the unparalleled development of Internet, the capabilities of telecommunication channels currently in use are quickly being pushed to its limits. It is impractical to replace all the telecommunication optical fibers installed with new fibers of more channels. And the unpredictable development may soon outdate these new fibers within two or three years. To maximize the usage of the currently installed optical fibers, the WDM scheme is gaining popularity for multiplacating the communication capacity of currently installed fibers. The idea is simply to divide the information to be transferred, and encode it into optical channels of different wavelength. However, these wavelength must be in the attenuation windows of the fibers, say the 1.55 μm range. The wavelengthes available are thus strictly restricted due to the requirement of minimum separation between channels for limiting crosstalk between different channels. With current technology the the separation of the channel is about 1.6 nm, and the bandwidth of each channel should be no less than 0.5 nm. To achieve such stringent requirements, the design of optical device is facing significant challenges.

In particular, the add-drop process in the WDM scenario challenges the current optical filter technology. It is desirable to have lower insertion loss and flat-top transfer function with sharp edges and ultra-narrow passband width. The PBG materials provide a new solution to WDM filters, as first proposed by Fan *et. al.*[7]. The processes occur between two waveguides side coupled through a resonator system. The resonator system is composed of microcavities formed by producing defects in the photonic crystals. The optimal channal drop is achieved when a signal with pre-selected frequency associated with the resonator system is completely transferred from one waveguide to the other, with all the other signals unchanged. By deliberate design of the resonator system utilizing photonic crystal, 99% transfer efficiency[7, 8] has been demonstated in numerical calculations. One assumption in the modeling of the channel drop filter was that the guiding states in two waveguides

do not interact with each other[8]. However, to make the resonator system couple to the waveguide, there must be some leakage of the wave amplitude into the crystal. Part of the leaking amplitude will coupled with states in the other waveguide. Such coupling may result in effective interaction comparable to that due to the indirect coupling through the resonator system. Therefore, such coupling is not negligible. To study the case when such direct interaction is present, we introduce the full symmetrized states of the two waveguide system, and study the cases of resonator systems composed of two localized states and four localized states. We show the general quality and line shape of the tranfer functions are not significantly affected by the presence of the direct coupling, which is in agreement with the result of numerical calculation. Furthermore, we find that we can achieve better flattop transfer function by enhancing the symmetry of the system. Fan *et. al.* proposed to increase the number of localized states to achieve better flattop, but without symmetry, they did not obtain any useful result due to difficulty of decoupling localized states. Enhancement of the system symmetry implies raising not only the symmetry of the localized states, but that of the waveguides as well. In this thesis, we propose a system with 3-fold symmetry with 3 waveguides and 6 cavities. This system gives a higher order flat-top transfer function with the denominator in 6th power of frequency. The enhancement of symmetry gives new latitude for shaping the transfer function by providing an optimization parameter. The empirical optimal value for this parameter is found in this thesis by an extensive investigation of various cases.

Further application of photonic crystal will emerge as the study of photonic crystal step forward. The range of application of photonic crystal in the information age is only limited by the imagination of human minds.

C. Localization of Light in Photonic Crystal

Another clue of the study of photonic crystal is the theorectical study of localization.

Following the pioneering steps of P. W. Anderson[9] and N. F. Mott[10], numerous re-

searchers have devoted the study and observation to the electron localization in disordered solids. Some general features of localization are well estabished now[11]. However, due to the existence of electron-electron interaction and electron-phonon interaction, theoretical predictions often meet with difficulties in definitively accounting for the experimental data. S. John first explored the possibility of observing localized states of light in a dielectric medium[2], in which the complication of the interactions associated with electrons are avoided so the further study of localization[12] in such systems is facilitated. Experiments quickly verified the existence of weak localization in the form of coherent backscattering [13]. However, for the implementation of strong localization of light, there is another serious problem: the effective energy of the wave equation of light in an inhomogeneous medium is always positive, and even worse, the energy of the photons is always higher than the potential barriers[14]! After Yablonovitch first proposed a three-dimensional dielectric structure with Photonic Band Gaps (PBG), John recognized[15] that a moderate disordered perturbation of this structure may provide the key to the predictable and systematic observation of strong localization of light. The gist of his theory is that the underlying superlattice provides a band gap for the frequency range of localization because of the remnant geometric Bragg resonances. Though studies along this theoretical line [16, 17, 18] have been carried out by several groups, some fundamental questions have remained unsolved as discussed below. Many studies (experimental and theoretical) have been conducted on the disorder in a homogeneous background[19, 20], instead of in a superlattice. Their results can not be generalized to localization in PBG materials because of the absence of Bragg scattering in the homogeneous background. Therefore the problem of strong localization in moderately disordered lattice is far from fully understood. For example, the only known embodiment of the "interplay between order and disorder"[15] is that localization is present at moderate, rather than at high degree of disorder, but will this interplay bring some other drastic changes to the whole picture of localization? Further, John has argued that the localization mechanism due to the remnant geometric Bragg resonances in dielectric structure is a new one[15]. Then the question remains whether the localization mechanism with which we are

familiar in Anderson model is also present in a dielectric structure? If it is, how will these two mechanisms interact with each other, and what interesting consequences will the coexistence of these two mechanisms bring? These questions will be addressed in the last part of the report. This part was also published in Physical Review B in November 1999. [21]

Finally in this introduction, we emphasize that with the fast development of telecommunication, particularly the Internet, the advantage of optical devices will become more and more obvious over the traditional electronic device. The perfect confinement capability of the photonic crystal is the key for its crucial role in this new Internet century. Nonetheless there are many problems and applications to be studied for PBG materials. The problems studied in this report reflect the recent trend in the study of PBG materials.

II. DISPERSION RELATION OF 2-D WAVEGUIDES

A. Description of the Problem

The photonic crystal behaves like a perfect mirror for light with frequency lying inside the bandgap. Suppose we drill a line defect through the crystal. When a light is sent into this line defect, due to perfect internal reflection, it will be guided through this line defect until it propagates out of the crystal. Unlike in the case of fibers, the internal reflection extends to any incident angle at the guide-crystal boundary, therefore provides much flexibility of designing the guide. A particular case is to use the photonic crystal to guide light around sharp corners.[4] It is shown the efficiency is higher than 95% where the performance of the traditional waveguide is very poor. However, a full of theoretical treatment of the dispersion relation is not seen in the literature. There are some numerical results for some specific systems[4]. Also, some empirical formulae are found for some systems based on the experimental data.[22, 23] In this chapter, we proposed a theory of dispersion relation for PBG materials-based waveguides.

FIGURES

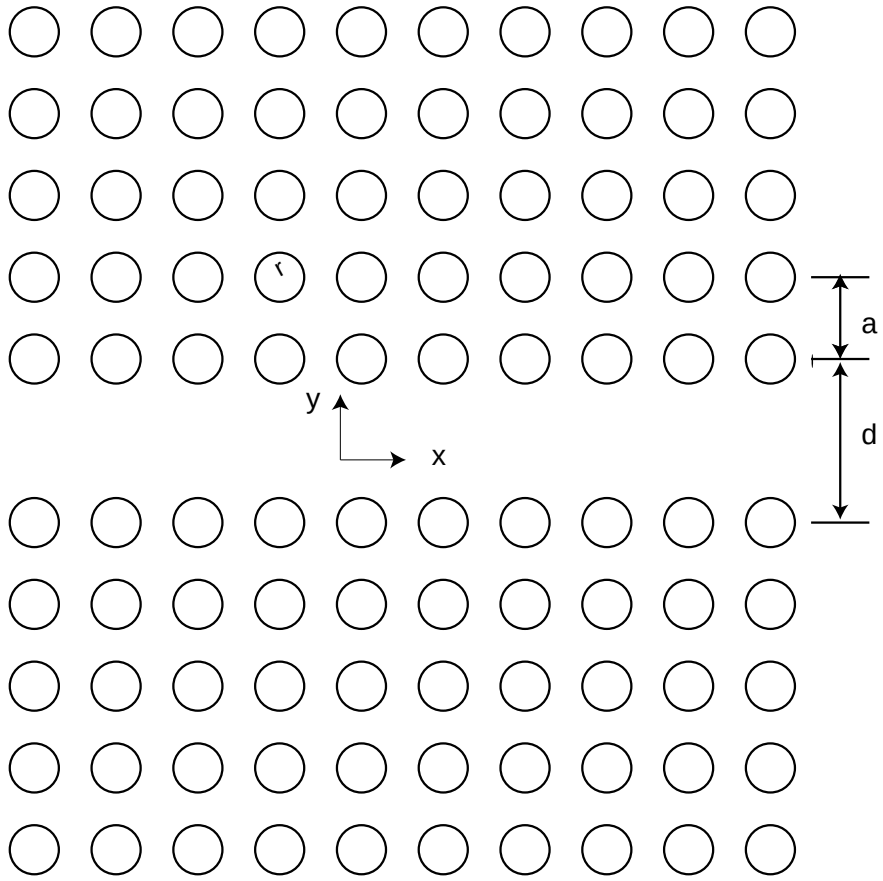

Fig. 1

Consider the case of the two-dimensional(2-D) crystal structure shown in Fig. 1, which has been investigated extensively in both theoretical[4, 7, 8] and experimental[5] study. The corresponding band structure(for the lowest band) is shown is Fig. 2 with the first Brillouin zone. For simplicity, only the lowest TM band which most analysis is concentrated on is shown. A line defect is created by removing a row of rods inside the otherwise perfect crystal.

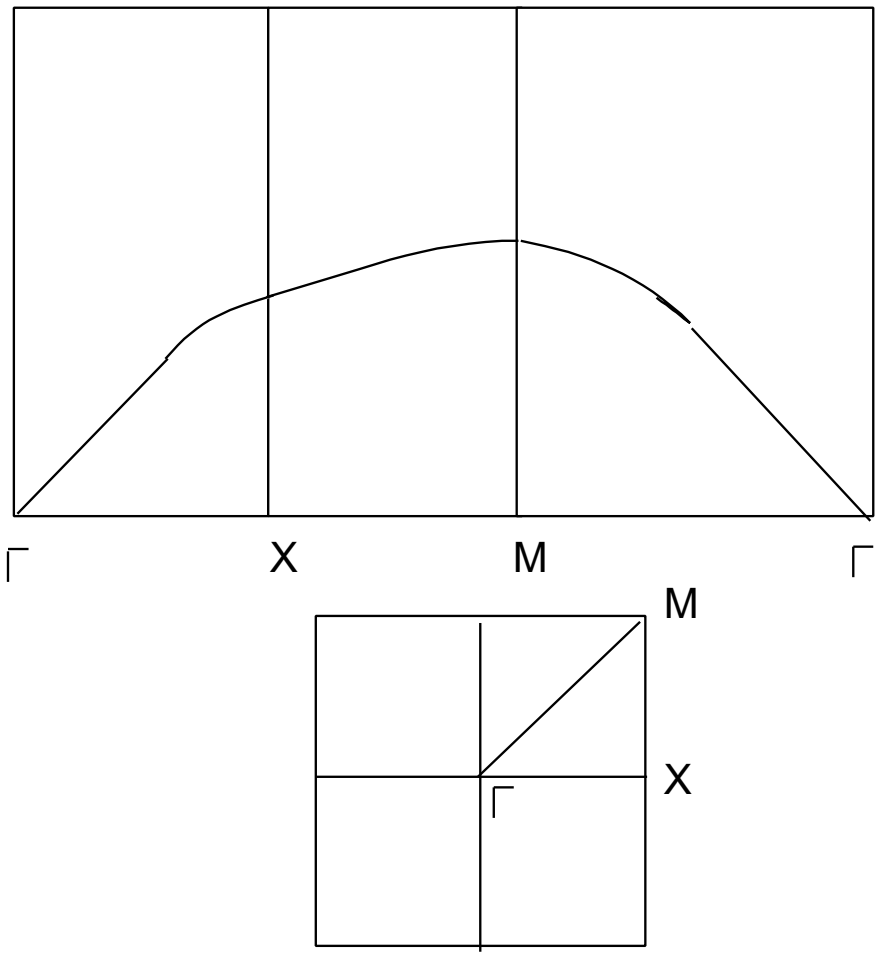

Fig. 2

The translational symmetry along the line defect allows the guided mode to be descibed with the quantum number k the wave vector and its frequency ω. The dispersional relation between ω and k calculated by numerical simulation is shown in Fig. 3(from Ref. [4], by the permission of Dr. S. Fan).

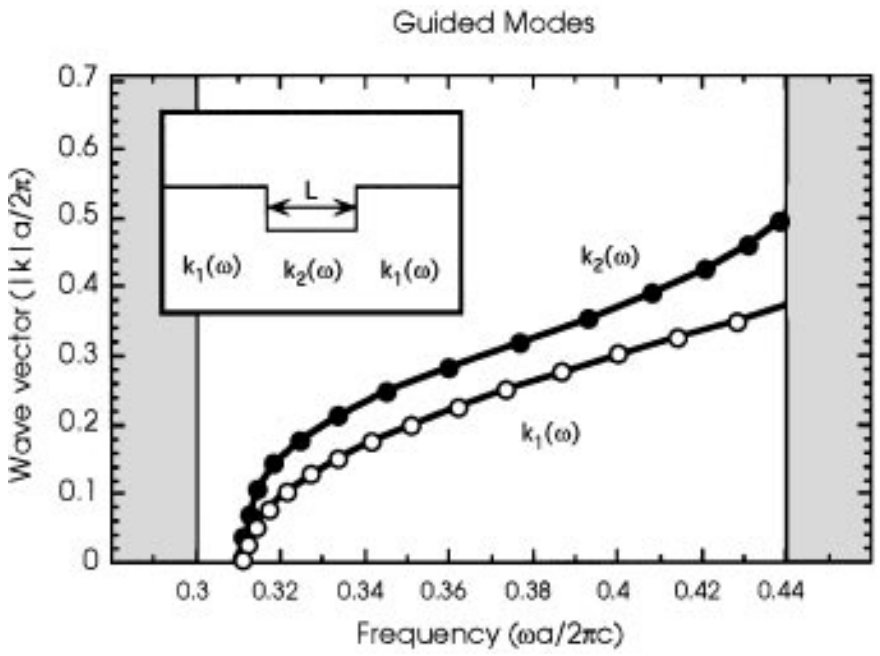

Fig. 3

Typically, to calculate this dispersion relation, one needs to simulate with a large scale computational cell (in Ref. [4], consisting of about 100×100 unit cells). Analytical study of this problem has not been reported. The difficulty lies in the fact that the electric field in the crystal is very complicated and an analytic solution is impossible for most cases. Therefore, though we know the mode profile in the guided region is propagating wave in the longitudinal direction and standing wave in the lateral direction, we can not yet match the electric field at the guide-crystal boundary due to lack of information of the electric field in the crystal. However, if we assume the band calculation of the perfect crystal is accomplished, by employing perturbation theory, we find there is a way to solve for the dispersion relation with all the parameters can be read from the band diagram. Note that the calculation of the band structure for a perfect crystal is performed in a single unit cell and is available for most structures of the photonic crystals which have been investigated. Therefore, the computational effort is considerably reduced. Furthermore, when the width or orientation of the line defect is changed, another simulation is needed to calculate the dispersion relation again. The analytic theory presented below just change to use the parameter at another

location of the band diagram of the same perfect crystal. It does not require another large scale simulation.

B. Band Folding

Simulation reveals the dispersion for crystal has the form shown in Fig. 3. For frequency below the lower edge ω of the band gap, no guided mode can propagate in the guide without significant loss. When ω increases from the lower edge of the band gap, a mode is present, and the wave vector this mode increases from zero in a nonlinear manner. For the crystal shown in Fig. 1 the correponding band diagram is shown in the Fig. 2. The band maximum is at the M point. The Bloch theorem yields the following form of the magnetic field in the crystal.

$$H = e^{ik_x x + ik_y y} U(x, y) \tag{2.1}$$

with the frequency for states near the band maximum M point given by

$$\omega^2 = \omega_0^2 + b(\mathbf{k} - \mathbf{k}_M)^2 \tag{2.2}$$

where $\mathbf{k} = (k_x, k_y)$ and $\mathbf{k}_M = (\frac{\pi}{a}, \frac{\pi}{a})$, a is the lattice constant. For the case of waveguide shown in Fig. 1, inside the crystal region, $k_y = i\gamma$ must be pure imaginary while k_x should be equal to the longitudinal wave vector in the guided region (air region), due to matching the paralell electric field(TE) or parallel magnetic field(TM) at the guide-crystal boundary. As the frequency tends to ω_0, one expects k_x and γ tend to zero. However, due to the presence of $\mathbf{k}_M$, these values can not satisfies Eq. (2.2). To clarify this paradox, we introduce the concept of band folding. In the spirit of nearly free electron approximation, we can perform the average of the periodic part of electromagnetic field $U(x, y)$ or equivalently assume it is constant throughout the space. It does not matter whether the average is performed in every one unit cell, or every two unit cells, as far as it is averaged over integer number of unit cells. However, if it is averaged over every two unit cells, we are effectively examining

a periodic structure not with a lattice constant a but $2a$. For this structure, the Brillouin zone is reduced to one quarter of the original area. The original M point is moved back to overlap with the Γ point. The boundary of the new Brillouin zone is indicate by primed characters X' and M' in Fig. 4.

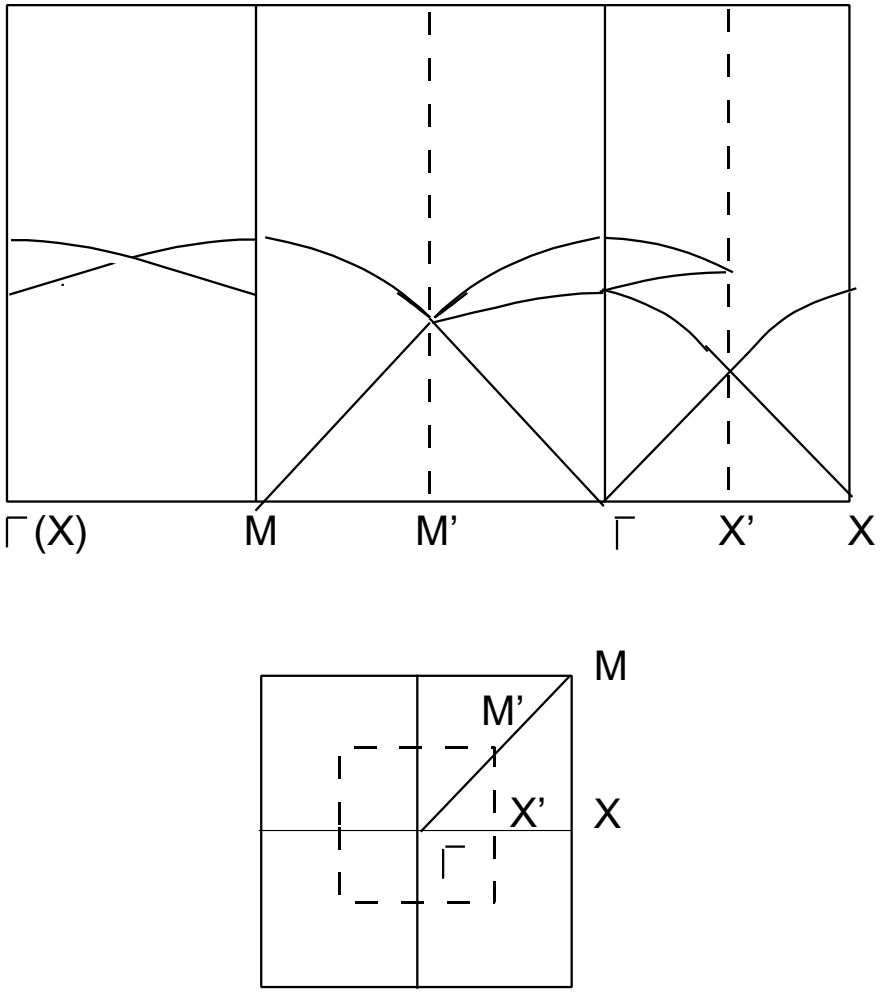

Fig. 4

The band maximum of the corresponding band structure is now located at the Γ point due to the folding of MM' to $\Gamma M'$ and $X'X$ to $X'\Gamma$. Note that the section of XM is also folded into the new first Brillouin zone. Now the band structure near the band maximum at the new Γ point is given by $\omega^2 = \omega_0^2 + bk^2$, for small $\mathbf{k}$, ω tends to ω_0.

C. Perturbation Theory of the Dispersion Relation

The Maxwell equations involved in the analysis are

$$\nabla \times \mathbf{E} = -\frac{\partial \mathbf{B}}{\partial t} \tag{2.3a}$$

$$\nabla \times \mathbf{H} = \frac{\partial \mathbf{D}}{\partial t} \tag{2.3b}$$

For convenience, let $\mu_0 = \epsilon_0 = c = 1$ in this report. For TM mode, the electric field is along the z direction for the two-dimensional crystal. The other components vanish. It is convenient to solve for the equation of electric field, which is a "scalar" equation,

$$-\nabla^2 E = \epsilon \omega^2 E \tag{2.4}$$

where $\epsilon = \epsilon(\mathbf{r})$ is the relative dielectric constant, which is a function of position.We have used the transver field condition $\nabla \cdot \mathbf{E} = 0$. Similarly, for TE mode, the magnetic field H has only one non-zero component along z. For this mode, it is convenient to solve the equation of the magnetic field

$$-\nabla(\frac{1}{\epsilon}\nabla H) = \omega^2 H \tag{2.5}$$

Because most simulation and experiments are done with the TM mode, we will examine it first.

For the configuration shown in Fig. (??), the wave is propagating along the x direction (in the terminology of two-dimensional Miller index, along the (10) direction), and the origin of the y axis is at the center of the waveguide. At the guide-crystal boundary, one must have $E \equiv E_z$ and H_x continuous. For a wave with frequency ω,

$$H_x = \frac{1}{i\omega}\frac{\partial E}{\partial y} \tag{2.6}$$

A more convenient choice of boundary condition is the continuity of the $\frac{1}{E}\frac{\partial E}{\partial y} \sim \frac{H_x}{E_z}$.

In the guided region, the mode profile is

$$E = \begin{cases} Ae^{ik_x x}\cos k_y y, & \text{even mode} \\ Ae^{ik_x x}\sin k_y y, & \text{odd mode} \end{cases} \tag{2.7}$$

Then at the boundary, the relative derivative of the electric field is

$$\frac{1}{E}\frac{\partial E}{\partial y} = \begin{cases} -k_y \tan k_y \frac{d}{2}, & \text{even mode;} \\ k_y \cot k_y \frac{d}{2}, & \text{odd mode.} \end{cases} \tag{2.8}$$

In crystal, due to symmetry in the y direction, one needs to consider the boundary condition only on one side of the guide, being either $y = \frac{d}{2}$ or $y = -\frac{d}{2}$. For convenience, we choose $y = \frac{d}{2}$. In the right half crystal, the electric field is given by

$$E(x, y) = e^{ik_x x}e^{-\gamma y}U(x, y) \tag{2.9}$$

Substitute this back into Eq. (2.4), (from now on, write k_x as k for simplicity).

$$-\left[-k^2U + 2ik\partial U\partial x + \frac{\partial^2 U}{\partial x^2} + \gamma^2 U - 2\gamma\frac{\partial U}{\partial y} + \frac{\partial^2 U}{\partial y^2}\right] = \epsilon\omega^2 U \tag{2.10}$$

The solution of this equation gives a family of function parameterized by (k, γ) We assume that the $U(x, y)$ has the form for small k and γ

$$U(x, y) = v(x, y)\,[1 + p(x)]\,[1 + q(y)] \tag{2.11}$$

where $p(x)$ is of the order of k and $q(y)$ is of the order of γ. Then the relative derivative of electric field at the boundary is

$$\begin{aligned} \frac{1}{E}\frac{\partial E}{\partial y} &= -\gamma + \frac{\partial}{\partial y}\ln v + \frac{\partial}{\partial y}\ln[1 + q] \\ &\cong -\gamma + \frac{v_y}{v} + q_y \end{aligned} \tag{2.12}$$

where the subscript y indicates partial derivative with respect to y.

We find that q_y can be expressed in terms of $\frac{v_y}{v}$ by perturbation technique. The equations in first and second orders of γ are

$$2\gamma\frac{\partial v}{\partial y} - \frac{\partial^2(qv)}{\partial y^2} = \epsilon\omega_0^2 qv \tag{2.13a}$$

$$-\left[\gamma^2 v - 2\gamma\frac{\partial}{\partial y}(qv)\right] = \epsilon b\gamma^2 v \tag{2.13b}$$

From Eq. (2.13b), we have

$$\frac{\partial}{\partial y}(qv) = \frac{1+b\epsilon}{2}\gamma v \tag{2.14}$$

Substitute it back into Eq. (2.13a) gives

$$q = \frac{\gamma}{2\epsilon\omega_0^2}\left[3-b\epsilon\right]\frac{v_y}{v} \tag{2.15}$$

By virtue of Eq. (2.13b), one finds

$$q_y = \frac{1+b\epsilon}{2}\gamma - \frac{\gamma}{2\epsilon\omega_0^2}\left[3-b\epsilon\right](\frac{v_y}{v})^2 \tag{2.16}$$

Therefore, the matching of the relative derivative of electric field at the boundary gives

$$k_y \tan k_y\frac{d}{2} = -\frac{v_y}{v} + \gamma\left[\frac{1-b\epsilon}{2} + \frac{1}{2\epsilon\omega_0^2}(3-b\epsilon)(\frac{v_y}{v})^2\right] \tag{2.17}$$

where $\frac{v_y}{v}$ is evalutated at the boundary $y = \frac{d}{2}$. Note that in the guided region, k_y is given by

$$k_y = \sqrt{\omega^2 - k_x^2} \tag{2.18}$$

while in the crystal, γ is given by

$$\gamma = \sqrt{\frac{\omega^2-\omega_0^2}{b} + k_x^2} \tag{2.19}$$

The quantity $\frac{v_y}{v}$ can be determined from the requirement that $k_x = 0$ at $\omega = \omega_0$. Therefore, $\frac{v_y}{v} = -\omega_0 \tan(\omega_0\frac{d}{2})$. The parameters ω_0 and b can be determined from the band diagram. The calculated dispersion relation is shown in Fig. 5.

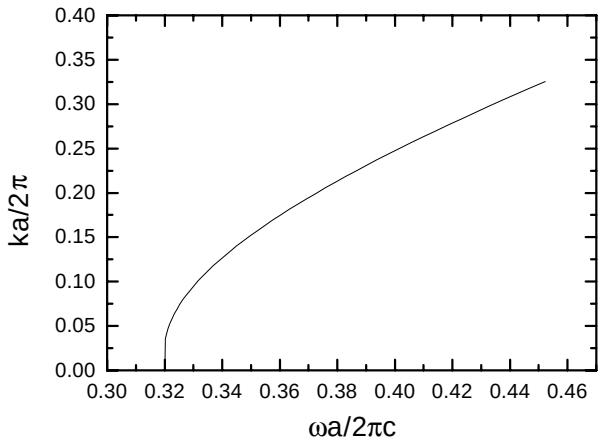

Fig. 5

Compared with the results obtained from numerical calculation[5] it agrees well when ω is not far above ω_0 as expected. When the ω approach the upper edge of the gap, there can be about 20% difference between the analytic and numerical results. Another problem is that our theory finds k_x is not zero though pretty small (0.035) at the lower edge of the gap. This is a well-understood phenomenon in 1-D wavegides or fibers[24] and is also observed in experiments for photonic crystal based waveguides.[23] However, the numerical calculation by Villeneuve *et. al.* [5] showed it was zero. In next chapter, we will discuss this problem in details. For odd TM mode

$$\begin{aligned} k_y \cot k_y \frac{d}{2} &= \frac{v_y}{v} - \gamma \left[\frac{1-b\epsilon}{2} + \frac{1}{2\epsilon\omega_0^2}(3-b\epsilon)(\frac{v_y}{v})^2 \right] \\ \frac{v_y}{v} &= \omega_0 \cot \omega_0 \frac{d}{2} \end{aligned} \tag{2.20}$$

For the TE mode, note that ϵ is constant in each region, then the above arguments applies also to this case. From Eq. (2.3b)

$$\frac{1}{\epsilon H}\frac{\partial H}{\partial y} = -i\omega \frac{E_x}{H_z} \tag{2.21}$$

should be continuous (Note H is just H_z). Then the boundary condition yields that for even mode (even in magnetic field, not electric field) and odd mode

$$k_y \tan k_y \frac{d}{2} = -\frac{1}{\epsilon}\frac{v_y}{v} + \frac{\gamma}{\epsilon}\left[\frac{1-b\epsilon}{2} + \frac{1}{2\epsilon\omega^2}(3-b\epsilon)(\frac{v_y}{v})^2 \right], \quad H\ even \tag{2.22}$$

$$k_y \cot k_y \frac{d}{2} = \frac{1}{\epsilon}\frac{v_y}{v} - \frac{\gamma}{\epsilon}\left[\frac{1-b\epsilon}{2} + \frac{1}{2\epsilon\omega^2}(3-b\epsilon)(\frac{v_y}{v})^2 \right], \quad H\ odd \tag{2.23}$$

III. DISPERSION RELATION OF 1-D WAVEGUIDES

It is of general interest to investigate the propagation of light in one-dimensional photonic crystal, and imperfect one-dimensional crystal(1-D waveguide). The frequency spectrum of the one- dimensional crystal is exactly solvable based on Bloch Theorem. We will see in many cases the scattering model in one-dimensional photonic crystal can also be solved exactly.

A 1-D photonic crystal is composed of an infinite array of dielectric slabs parallel to the XZ. The slabs have thickness b, while the air gaps between the slabs have thickness d. The periodicity of the photonic crystal is $a = b + d$. The dielectric constant of the slabs are assumed to be ϵ. For the TE mode, the electric field is in the z direction. The wavevector k is normal to the slabs in the y direction for 1-D problem, while for semi 1-D problem, the k vector lies in the XY plane, and still perpendicular to the wavevector.

A. The Frequency Spectrum

The wave equation for TE mode is given by

$$-\nabla^2 E = \epsilon(y)\omega^2 E(x, y) \tag{3.1}$$

The continuity of tangential electric field and magnetic field at the interfaces of between slabs and air gives the boundary conditions. Note for a mono-chromatic field, the Maxwell equation for curl of the electric field gives the tangential magnetic field H_x is proportional to the partial derivative of the electric field with respect to y. Therefore, at the slab-air boundary, the boundary condition is simply that the electric field and its normal derivative is continuous. Assume in the slab region between $y = 0$ and $y = b$, the electric field is given by

$$e^{ik_x x}(Ae^{i\beta y} + Be^{-i\beta y}) \tag{3.2}$$

where k_x and β are x and y components of the wave vector, respectively. In the air region between $y = b$ and $y = a$, the electric field is

$$e^{ik_x x}(Ce^{ik_y y} + De^{-ik_y y}) \tag{3.3}$$

where k_x and β are x and y components of the wave vector,

where k_y is the y component of the wave vector in this region. The x component of the wave vector must be the same in two regions as follows from the continuity of the normal component of the magnetic field.

The boundary conditions lead to the following equations

$$\begin{aligned} Ae^{i\beta b} + Be^{-i\beta b} &= Ce^{ik_y b} + De^{-ik_y b} \\ Ae^{i\beta b} - Be^{-i\beta b} &= \frac{k_y}{\beta}(Ce^{ik_y b} - De^{-ik_y b}) \\ \lambda(A+B) &= Ce^{ik_y a} + De^{-ik_y a} \\ \lambda(A-B) &= \frac{k_y}{\beta}(Ce^{ik_y a} - De^{-ik_y a}) \end{aligned} \tag{3.4}$$

The last two equations are due to Bloch theorem and $\lambda = e^{-i\overline{k}a}$, $\overline{k}$ is the reduced wave vector. Solve these equations, one finds the equation for λ is given by

$$\lambda^2 - 2f\lambda + 1 = 0 \tag{3.5}$$

where $f(\omega, k_x)$ is a function of frequency and x component of the wave vector.

$$f(\omega, k_x) = \cos\beta b \cos k_y d - \frac{k_y^2 + \beta^2}{2k_y\beta} \sin\beta b \sin k_y d \tag{3.6}$$

Note $k_y = \sqrt{\omega^2 - k_x^2}$ and $\beta = \sqrt{\epsilon\omega^2 - k_x^2}$. The solution is obvious

$$\lambda = f \pm \sqrt{f^2 - 1} \tag{3.7}$$

Therefore, λ is also a function of frequency and the x component of the wave vector.

Now consider the semi 1-D waveguide made up of an air "defect" of thickness w between $y = -w$ and $y = 0$. According to our 2-D theory, the only quantity we need to match at $y = 0$ is

$$\frac{1}{E}\frac{\partial E}{\partial y} = i\beta\frac{A-B}{A+B} \tag{3.8}$$

A straightforward but lengthy calculation gives

$$\frac{1}{E}\frac{\partial E}{\partial y} = -i\beta\frac{1-\lambda e^{-i\beta b}(\cos k_y d - i\frac{k_y}{\beta}\sin k_y d}{1-\lambda e^{-i\beta b}(\cos k_y d - i\frac{\beta}{k_y}\sin k_y d} \tag{3.9}$$

Now we note at the boundary π/a of the Brillouin zone, $\lambda = -1$. For frequency a little above lower edge of the pseudo gap, λ is given by $\lambda = e^{-\gamma a} = -1 + \gamma a$

Then the logarithmic derivative of the electric field is given by

$$\frac{1}{E}\frac{\partial E}{\partial y} = -\beta\frac{\sin\beta b\cos k_y d + \frac{k_y}{\beta}\cos\beta b\sin k_y d}{1+\cos\beta b\cos k_y d - \frac{\beta}{k_y}\sin\beta b\sin k_y d} + \gamma\frac{\beta a\left(\sin\beta b\cos k_y d + \frac{k_y}{\beta}\cos\beta b\sin k_y d\right)}{\left(1+\cos\beta b\cos k_y d - \frac{\beta}{k_y}\sin\beta b\sin k_y d\right)^2} \tag{3.10}$$

On the other hand, the frequency has the following expansion at the near the edge of Brillouin zone

$$\omega^2 = \omega_0^2 + g\gamma^2 \tag{3.11}$$

where $g = -\omega_0 a^2/f'(\omega_0)$. According to 2-D theory,

$$\frac{1}{E}\frac{\partial E}{\partial y} = \left(\frac{1}{E}\frac{\partial E}{\partial y}\right)_0 - \gamma\left[\frac{1-g\epsilon}{2} + \frac{1}{2\epsilon\omega_0^2}(3-g\epsilon)\left(\frac{1}{E}\frac{\partial E}{\partial y}\right)_0^2\right] \tag{3.12}$$

The comparison of the result of the two formula is drawn in Fig. 6 for several typical values of ϵ and b.

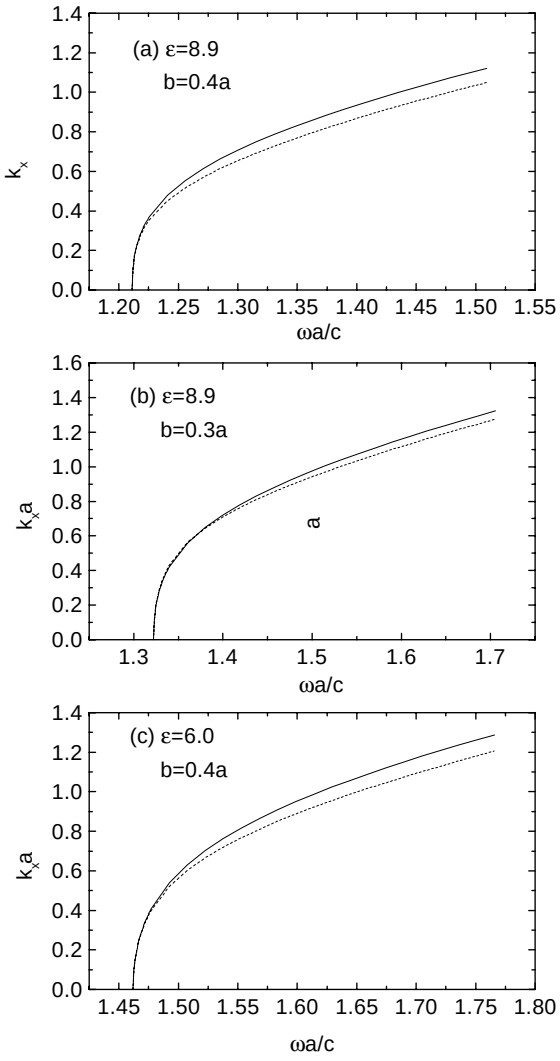

Fig. 6

For each case, we calculate from the lower edge of the gap up to the frequency corresponding to one third of the gap. The error is less than 7% for all the cases. One thing we needs to mention is that there may not be a propagating mode immediately above the lower edge of gap for a specific width of guided region(no matter using exact solution or our perturbation theory), as well-known in all kinds of 1-D waveguides and optical fibers.[24] Or the reverse case, there is a propagating mode, but its k_x is not zero, which means the propagating mode with $k_x = 0$ lies in the band. Though we can use the equations given above to find the dispersion relation for the modes with frequencies lying in the band, they have significant loss and are not useful. In Fig. 6, we just picked the width of waveguide to make the point where $k_x = 0$ coinciding with the lower edge of the gap for comparison with

2-D theory. For the cases where this is not true, the theory gives the same error percentage for the same frequency range, compared the exact theory. When the original gap is small, say the gap vs. midgap ratio is less than 0.5, the result of this theory is not good.

B. Pseudo Light Ray Method

The propagation of the wave in the waveguide is a dynamic process. The better formulation for such a process is scattering theory. In the semi 1-D system treated here, it can be cast into a theory of light rays.

To obtain an intuitive insight into the light ray method, let consider the following problem, as shown in Fig. 7.

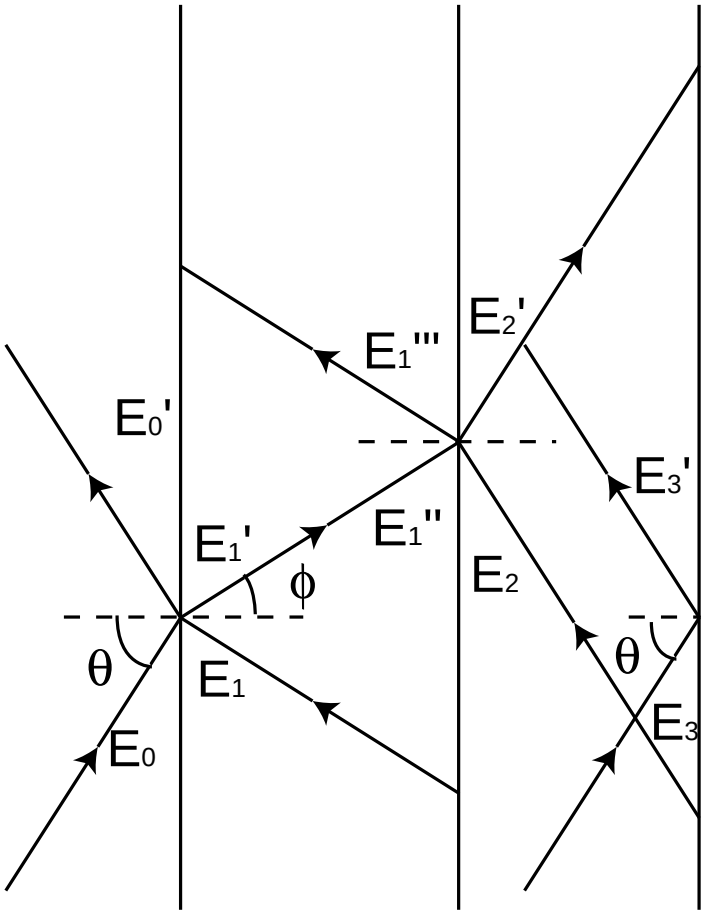

Fig. 7

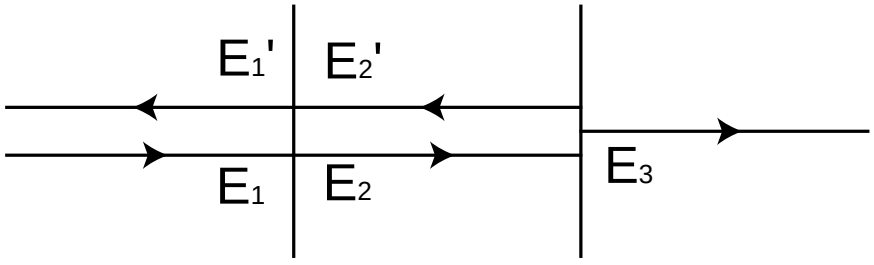

Fig. 8

In the 1-D crystal, a light ray with electric field E_0 is incident on the surface of one slab and is reflected with electric field E_0' from the air region. The incident angle is θ. Inside the slab, at the same point, another light ray E_1 is incident with angle ϕ on the interface and is reflected as E_1'. The continuity of tangential electric and magnetic field gives

$$E_0 + E_0' = E_1 + E_1' \tag{3.13}$$

$$-(H_0 - H_0')\cos\theta = (H_1 - H_1')\cos\phi \tag{3.14}$$

Note Maxwell equation gives $H = \frac{n}{\mu_0 c}E$, one finds

$$E_1 = \frac{1}{2}E_0\left(1 - \frac{\cos\theta}{n\cos\phi}\right) + \frac{1}{2}E_0'\left(1 + \frac{\cos\theta}{n\cos\phi}\right) \tag{3.15}$$

$$E_1' = \frac{1}{2}E_0\left(1 + \frac{\cos\theta}{n\cos\phi}\right) + \frac{1}{2}E_0'\left(1 - \frac{\cos\theta}{n\cos\phi}\right) \tag{3.16}$$

The reflected ray is incident on the other interface of the slab as E_1'' and is further reflected to be E_1'''. The amplitude of E_1'' is just E_1' multiplying a phase factor corresponding to the path. The amplitude of E_1''' is assumed to be related to ray E_1 parallel to it by the following rule. On any two parallel rays, every pair of points which have the same y and z coordinates but different x coordinates x_1 and x_1''', the relative amplitude of E_1''' ray to E_1 ray is $e^{ik_x(x_1''' - x_1)}$. The boundary condition at the second interface now can be written as

$$E_1' e^{inkb/\cos\phi} + E_1 e^{-inkb/\cos\phi + 2ik_x b\tan\phi} = E_2 + E_2' \tag{3.17}$$

$$(-H_1' e^{inkb/\cos\phi} + H_1 e^{-inkb/\cos\phi + 2ik_x b\tan\phi})\cos\phi = (H_2 - H_2')\cos\theta \tag{3.18}$$

The solution for E_2 and E_2' is

$$E_2 = \frac{1}{2}E_1 e^{-inkb/\cos\phi + 2ik_x b\tan\phi}\left(1 + \frac{n\cos\phi}{\cos\theta}\right) + \frac{1}{2}E_1' e^{inkb/\cos\phi}\left(1 - \frac{n\cos\phi}{\cos\theta}\right) \tag{3.19}$$

$$E_2' = \frac{1}{2}E_1 e^{-inkb/\cos\phi + 2ik_x b\tan\phi}\left(1 - \frac{n\cos\phi}{\cos\theta}\right) + \frac{1}{2}E_1' e^{inkb/\cos\phi}\left(1 + \frac{n\cos\phi}{\cos\theta}\right) \tag{3.20}$$

According to the rule for determining the relative amplitude of two parallel rays, the amplitude of two rays E_3 and E_3' incident and reflected, respectively, at point P are given in terms of E_2 and E_2' by

$$E_3 = E_2' e^{ikd/\cos\theta - ik_x(b\tan\phi + d\tan\theta)} \tag{3.21}$$

$$E_3' = E_2 e^{-ikd/\cos\theta - ik_x(b\tan\phi - d\tan\theta)} \tag{3.22}$$

Therefore, they are related to E_0 and E_0' as follows

$$\begin{aligned} E_3 = & \frac{1}{4}e_2^+ \left[e_1^-(1-\frac{1}{r_t})(1-r_t) + e_1^+(1+\frac{1}{r_t})(1+r_t) \right] E_0 \\ & + \frac{1}{4}e_2^+ \left[e_1^-(1-\frac{1}{r_t})(1+r_t) + e_1^+(1+\frac{1}{r_t})(1-r_t) \right] E_0' \end{aligned} \tag{3.23}$$

$$\begin{aligned} E_3' = & \frac{1}{4}e_2^- \left[e_1^-(1+\frac{1}{r_t})(1-r_t) + e_1^+(1-\frac{1}{r_t})(1+r_t) \right] E_0 \\ & + \frac{1}{4}e_2^+ \left[e_1^-(1+\frac{1}{r_t})(1+r_t) + e_1^+(1-\frac{1}{r_t})(1-r_t) \right] E_0' \end{aligned} \tag{3.24}$$

where

$$e_1^{\pm} = e^{\pm i(nkb/\cos\phi - k_x b\tan\phi)}$$

$$e_2^{\pm} = e^{\pm i(kd/\cos\theta - k_x d\tan\theta)}$$

These equations can be cast into matrix form

$$\begin{pmatrix} E_3 \\ E_3' \end{pmatrix} = \begin{pmatrix} a & b \\ c & d \end{pmatrix} \begin{pmatrix} E_0 \\ E_0' \end{pmatrix} \tag{3.25}$$

The eigenvalues of the 2×2 matrix satisfies

$$\lambda^2 - (a+d)\lambda + (ad - bd) = 0 \tag{3.26}$$

A lengthy calculation shows that

$$a + d = 2f(\omega, k_x),\ ad - bc = 1 \tag{3.27}$$

This is exactly the same as we got in the previous section. And one easily shows if roots of λ are complex (for perfect crystal), they appear in conjugate pairs and their moduli are 1. Therefore, E_0 and E_0' can be supposition of two eigenvectors corresponding to the two roots. For imperfect crystal, one roots corresponds to exponential growth in the $y > 0$ region and should be discarded. Therefore, the pair (E_0, E_0') is uniquely determined(up to a normalization factor).

C. Light Ray Method

Actually, the light ray theory given above are based on the standing waves, which are the coherent supposition of many travelling waves reflected back and forth in the crystal. Like the theory of stationary equations, it assumes a colliminated light beam of infinite width is incident on(or in) the crystal. It inherently can not deal with the problem of a beam of finite width incident on a crystal.

A TRUE light ray theory should start from the ananlysis of a single light ray with the rule we learn from the previous section: how to determine the relative amplitude of parallel rays.

The following formula for reflection and transmission coefficients is well-known in optics.

$$r = \frac{\cos\theta - n_r \cos\phi}{\cos\theta + n_r \cos\phi}, \quad t = \frac{2\cos\theta}{\cos\theta + n_r \cos\phi} \tag{3.28}$$

where n_r is the relative index of refraction of the material which the ray is incident on with respect to the medium the ray is travelling.

First, consider a single ray is incident on a dielectric slab from air. It is a trivial exercise to show that the reflected rays have amplitudes (assuming incident has unit amplitude), from left to right,

$$r, tr't'e^{2i\Delta}, tr't'e^{2i\Delta} \cdot \left(r'e^{2i\Delta}\right)^2, tr't'e^{2i\Delta} \cdot \left(r'e^{2i\Delta}\right)^4, ... \tag{3.29}$$

the transmitted rays on the other side have amplitudes

$$tt'e^{i\Delta}, tt'e^{i\Delta} \cdot \left(r'e^{2i\Delta}\right)^2, tt'e^{i\Delta} \cdot \left(r'e^{2i\Delta}\right)^4, ... \tag{3.30}$$

where r and t are given in Eq. (3.28), and

$$r = \frac{\cos\theta - n\cos\phi}{\cos\theta + n\cos\phi}, \quad t = \frac{2\cos\theta}{\cos\theta + n\cos\phi} \tag{3.31}$$

$$r' = \frac{\cos\phi - \frac{1}{n}\cos\theta}{\cos\phi + \frac{1}{n}\cos\theta}, \quad t' = \frac{2\cos\phi}{\cos\phi + \frac{1}{n}\cos\theta} \tag{3.32}$$

From these equations, we will develop a Green's function approach to light ray propagation. First, we associate each dielectric slab with a "potential"

$$V(x,y,s;x_0,y_0,s_0) = V_r(x,y;x_0,y_0)\delta_{s,-s_0} + V_t(x,y;x_0,y_0)\delta_{s,s_0} \tag{3.33}$$

where the reflection and transmission "potentials" are given by

$$\begin{aligned} V_r =& r\delta(x-x_0)\delta(y-y_0) \\ &+\delta(y-y_0)tr't'e^{2i\Delta}\sum_{n=0}^{\infty}\left(r'e^{i\Delta}\right)^{2n}\delta\left[x-(x_0+2(n+1)b\tan\phi)\right] \end{aligned} \tag{3.34}$$

$$V_t = \delta[y-(y_0+sb)]tt'e^{i\Delta}\sum_{n=0}^{\infty}\left(r'e^{i\Delta}\right)^{2n}\delta\left[x-(x_0+(2n+1)b\tan\phi)\right] \tag{3.35}$$

The subscripts s and s_0 indicate the sign of the y component of the correponding rays. To each air region, we associate it with a free space Green's function

$$G_0(x,y,s;x_0,y_0,s_0) = \delta\left[x-(x+d\tan\theta)\right]\delta\left[y-(y_0+sd)\right]e^{i\Delta'}\delta_{s,s_0} \tag{3.36}$$

where $\Delta' = kd/\cos\theta$.

The Green's functions for the photonic crystal is then given by

$$\begin{aligned} G(x,y,s;x_0,y_0,s_0) =& \delta(x-x_0)\delta(y-y_0)\delta_{s,s_0} \\ &+\int dx_1dy_1\sum_{s_1=0,1}G_0(x,y,s;x_1,y_1,s_1)V(x_1,y_1,s_1;x_0,y_0,s_0) \\ &+\int dx_1dy_1dx_2dy_2dx_3dy_3\sum_{s_1,s_2}G_0(x,y,s;x_3,y_3,s_3)V(x_3,y_3,s_3;x_2,y_2,s_2) \\ &\quad\times G_0(x_2,y_2,s_2;x_1,y_1,s_1)V(x_1,y_1,s_1;x_0,y_0,s_0) \\ &+\cdots \end{aligned} \tag{3.37}$$

The internal coordinates $x_1, y_1, x_2, y_2...$ are integrated over the space and the internal subscripts $s_1, s_2, s_3, ...$ are summed. From this Green's function, one can find the amplitude of all the rays at any interface generated from the single incident ray. Because it gives only the amplitude of rays at the interfaces, it is better called a reduced Green's functions. However, the calcultion of the field in other locations are straightforward(just a multiplication of some phase factor). V_r, V_t and G_0 has a compact intergral representation (Fourier Transform).

$$V_r = \int\frac{d^2q}{(2\pi)^2}e^{i\mathbf{q}(\mathbf{x}-\mathbf{x}_0)}\left[r+\frac{tr't'e^{2i\Delta-2iq_xb\tan\phi}}{1-\left(r'e^{i\Delta-iq_xb\tan\phi}\right)^2}\right] \tag{3.38}$$

$$V_t = \int \frac{d^2q}{(2\pi)^2} e^{i\mathbf{q}(\mathbf{x}-\mathbf{x}_0)} \frac{tt' e^{i\Delta - iq_x b\tan\phi - iq_y sb}}{1-\left(r' e^{i\Delta - iq_x b\tan\phi}\right)^2} \tag{3.39}$$

$$G_0 = \int \frac{d^2q}{(2\pi)^2} e^{i\mathbf{q}(\mathbf{x}-\mathbf{x}_0)} e^{i\Delta' - iq_x d\tan\theta - iq_y sd} \tag{3.40}$$

Now in pseudo wave vector $\mathbf{q}$ space, the Green's function is a sum of matrix products. Due to the subscripts $s, s_1, s_2, ..., s_0$, every free space Green's function and potential is a 2×2 matrix. Depending on the problems, one may restrict the summation to a series of specifice terms.

As an example, consider a light ray is normally incident on a slab, as shown in Fig. 8. Using stationary wave methods, we assume there are at most two waves in each region. The equations at the interfaces are

$$E_1 + E_1' = E_2 + E_2'$$

$$H_1 - H_1' = H_2 - H_2'$$

$$E_2 e^{i\Delta} + E_2' e^{-i\Delta} = E_3$$

$$H_2 e^{i\Delta} - H_2' e^{-i\Delta} = H_3$$

One easily finds the solutions for reflection and transmission coefficients

$$\frac{E_1'}{E_1} = \frac{(n^2-1)\left(e^{2i\Delta}-1\right)}{(n+1)^2 - (n-1)^2 e^{2i\Delta}}$$
$$\frac{E_3}{E_1} = \frac{4ne^{i\Delta}}{(n-1)^2 e^{2i\Delta} - (n+1)^2}$$

Now compared with the results given by V_r and V_t, (actually, they are just V_r and V_t evaluated at $\theta = \phi = 90^o$), they are exactly the same.

This theory can be applied to the problem of reflecting a beam with finite width at the surface of the photonic crystal. One will find that the reflecting light are not a uniform beam with finite width. The reflecting light will come out from any point of the surface with a non-uniform intensity.

IV. GROUP THEORY APPROACH OF CHANNEL DROP FILTERS

A. The Hamiltonian

The schematic diagram of a channel drop system is shown in Fig. 9(from Ref. [8], by the permission of Dr. S. Fan).

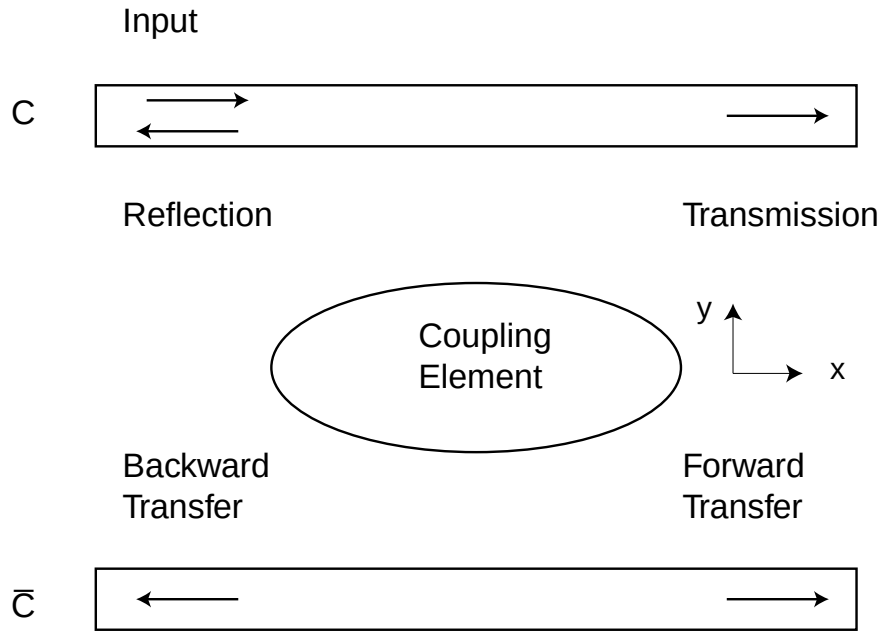

Fig. 9

The system is composed of two identical continuums, labled C and $\overline{C}$, side coupled through a resonator system. Following the notation of Fan et. al.,[8] states with a wave vector k in the two continuums are labled $|k\rangle$ and $|\overline{k}\rangle$, accordingly. The resonator system supports localized states, labled as $|c\rangle$. The complete Hamiltonian for such a system is

$$
\begin{aligned}
H &= H_0 + V \\
H_0 &= \sum_k \omega_k |k\rangle\langle k| + \sum_c \omega_c |c\rangle\langle c|, \\
V &= \frac{1}{L} \sum_{k_1 \neq k_2} V_{k_1,k_2} |k_1\rangle\langle k_2| + \sum_{c_1 \neq c_2} V_{c_1,c_2} |c_1\rangle\langle c_2| + \frac{1}{\sqrt{L}} \sum_{k,c} \left[V_{c,k} |c\rangle\langle k| + V_{k,c} |k\rangle\langle c| \right].
\end{aligned}
\tag{4.1}
$$

where ω_k is the frequency of the state $|k\rangle$, the interaction coefficient V_{ab} (a and b can be either localized or propagating states) satisfies the conjugate relation $V_{ab} = V_{ba}^*$. The sum over k includes two continuums. When V_{k_1,k_2} vanish, it reduces to the model proposed by Fan *et. al.* [7, 8] However, this coupling is generally not negligible. For example, we assume the exponential decay $e^{-\gamma_c r}$ for the wavefunction of the localized states and assume the lateral mode profile for a propagating mode in one waveguide also has the simply exponential form $e^{-\gamma_g |y|}$ in the crystal region. If γ_g is comparable to, or greater than γ_c, then the direct coupling can not be neglected! Therefore, a careful treatment of this kind of coupling is necessary.

When there is no such interaction, the Lippmann-Schwinger equation for this Hamiltonian can be solved at ease if there are only several localized states. The essence of the treatment is the reduction of the dimension of effective interaction matrix to the number of localized states. Generally, when the direct coupling is present, there is no such reduction. The problem becomes difficult to handle. However, we find if the two continuums are identical, then the interaction coefficients V_{k_1,k_2} are not zero only if $k_1 = \overline{k}_2$, which means k_1 and k_2 have the same magitude and sign except they are in different waveguides. This can be proved by noting the interaction coefficient is actually the overlap integral between the two states. If the number of defects(or more precisely the area of defect region) is finite, the integral for a system like shown in Fig. 10(from Ref. [8], by the permission of Dr. S. Fan) , differs from a system with complete translational symmetry in x direction (no defects or cavities) only by an amount of the order $\frac{area\ of\ the\ defects}{area\ of\ the\ system}$. As the area of the system goes to infinity, this term vanishes. And we know for a truly translational-symmetric system, two modes do not interacts if their longituding wavevector are different.

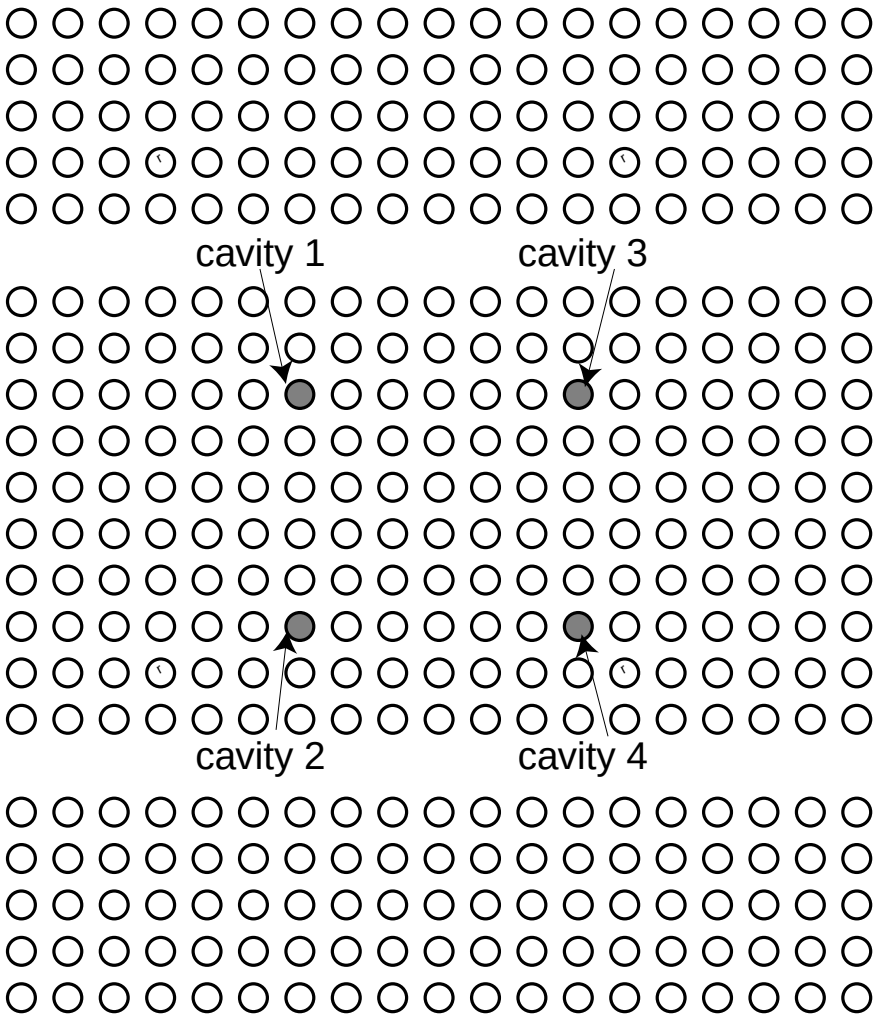

Fig. 10

By employing symmetry, we can renormalize the states of the two continuums into the following two kinds of states:

$$|ke\rangle = \frac{1}{\sqrt{2}}(|k\rangle + |\overline{k}\rangle), \tag{4.2a}$$

$$|ko\rangle = \frac{1}{\sqrt{2}}(|k\rangle - |\overline{k}\rangle), \tag{4.2b}$$

where e and o denotes the states having even or odd parity with respect to the mirror plane normal to y axis. Because of the symmetry of the system, the Hamiltonian commutes with the reflection with respect to the mirror plane perpendicular to y axis. There can not be

interaction between even and odd states. Therefore, in the new basis, the Hamiltonian has the form

$$\begin{aligned} H=& H_0 + V \\ H_0=& \sum_{k,\delta_y} \omega_{k,\delta_y} |k\delta_y\rangle\langle k\delta_y| + \sum_c \omega_c |c\rangle\langle c|, \\ V=& \sum_{c_1 \neq c_2} V_{c_1,c_2} |c_1\rangle\langle c_2| + \frac{1}{\sqrt{L}} \sum_{k,\delta_y,c} \left[V_{c,k\delta_y} |c\rangle\langle k\delta_y| + V_{k\delta_y,c} |k\delta_y\rangle\langle c| \right]. \end{aligned} \tag{4.3}$$

where the sum over δ_y includes the even and odd states.

B. Solve the Lippman-Schwinger Equation

To calculate the transmitted, transferred, or backscattered wave, one needs to solve the Lippman-Schwinger equation, which relates the scattered wave function $|\psi\rangle$ to the incoming wave $|k\rangle$

$$|\psi\rangle = |k\rangle + \frac{1}{\omega_k - H_0 + i\epsilon} V|\psi\rangle \equiv T|k\rangle \tag{4.4}$$

where ω_k is the frequency of the incoming wave (from now on, we use the k only to denote a propagating state and omit δ_y for convenience if there is no necessity of distinguishing the even and odd states), and ϵ is an infinitesimally small positive number introduced to enforce the outgoing boundary condition for the scattered wave.

The Lippman-Schwinger Equation can be solved iteratively. As a result, the T matrix can be represented as a sum of an infinite series

$$T_{k'k} = \sum_{m=0}^{\infty} \langle k'| \left(\frac{1}{\omega_k - H_0 + i\epsilon} V \right)^m |k\rangle \tag{4.5}$$

Since there is no direct coupling between the propagating states, it is possible to reduce the scattering process to the subspace spanned by the localized states. A fully diagramatic analysis (see Appendix A) gives the following form for the transition matrix

$$T_{k'k} = \delta_{k'k} + \frac{1}{\omega_k - \omega_{k'} + i\epsilon} \sum_{c_1,c_2} V_{k',c_2} G_{c_2,c_1}(\omega_k) V_{c_1,k} \tag{4.6}$$

where

$$G_{c_1,c_2}(\omega) = \langle c_2 | \frac{1}{\omega - H + i\epsilon} | c_1 \rangle \tag{4.7}$$

is the Green function in the subspace of localized states. The Green function has the standard form

$$G = (1 - G^0\Sigma)^{-1} G^0 \tag{4.8}$$

and G^0 and Σ are also in the subspace of the localized states. The unperturbed Green function is

$$G^0_{c_1,c_2}(\omega) = \frac{1}{\omega - \omega_{c_1} + i\epsilon} \delta_{c_1,c_2} \tag{4.9}$$

and the self-energy is summed exactly (see Appendix A) to be

$$\Sigma_{c_1,c_2} = V_{c_1,c_2} + \frac{1}{L} \sum_q V_{c_1,q} \frac{1}{\omega - \omega_q + i\epsilon} V_{q,c_2} \tag{4.10}$$

C. Two-Cavity Filter

Now consider the case where there are only two localized states, which are even and odd modes with respect to the mirror plane normal to x axis.

In the channel drop process, a light is injected into the upper continuum and is represented by Eq. (4.2a) Due to the mirror symmetry with respect to y axis, the two localized states must be either even or odd in y direction. When the two cavities are separate far from each other, the two cavities has only one mode, which should be either even or odd in y direction. This implies that the symmetrized modes of the two cavities should be either both even or both odd in y direction. For simplicity, we consider the case that they are both even first. One direct result is that only $|ke\rangle$ propagating states are scattered by the resonator system, or $V_{ko,e} = V_{ko,o} = 0$. Because

$$V_{e,-qe} = V_{e,qe}, \; V_{o,-qe} = V_{o,qe} \tag{4.11}$$

the off-diagonal element of the self-energy

$$\Sigma_{eo} = \frac{1}{2}\sum_{q} \frac{V_{e,qe}V_{qe,o} + V_{e,-qe}V_{-qe,o}}{\omega - \omega_{qe} + i\epsilon} = 0. \tag{4.12}$$

where $V_{ee} = V_{eo} = V_{oo} = 0$ after symmetrization due to the symmetry of the system. The diagonal element of the self-energy is given by

$$\begin{aligned}
\Sigma_{cc} &= \frac{1}{2\pi}\int \frac{dq}{d\omega_{qe}} d\omega_{qe} \frac{|V_{qe,c}|^2}{\omega - \omega_{qe} + i\epsilon} \\
&= \frac{\mathcal{P}}{2\pi}\int \frac{d\omega_{qe}}{g(\omega_q e)} \frac{|V_{qe,c}|^2}{\omega - \omega_{qe}} - i\frac{|V_{q(\omega)e,c}|^2}{g(\omega)} \\
&= -\Delta\omega_c - i\gamma_c
\end{aligned} \tag{4.13}$$

where the real part is the principle value of the integral. Now the Green function in the reduced space of the localized states is

$$G_{cc}(\omega) = \frac{1}{\omega - \widetilde{\omega}_c + i\gamma_c} \tag{4.14}$$

where $\widetilde{\omega}_c = \omega_c + \Delta\omega_c$. Now one easily sees that

$$\begin{aligned}
\langle x = \infty | T | ke \rangle &= \sum_{k'} \langle x = \infty | k'e \rangle \langle k'e | T | ke \rangle \\
&= \lim_{x\to\infty} \frac{L}{2\pi}\int dk' |e\rangle \frac{1}{\sqrt{L}} e^{ik'x} \left[\delta_{k'k} + \frac{1}{L} \frac{\sum_c V_{k'e,c} G_{cc} V_{c,ke}}{\omega_{ke} - \omega_{k'e} + i\epsilon} \right] \\
&= \lim_{x\to\infty} \frac{1}{\sqrt{L}} e^{ikx} |e\rangle \left[1 - \frac{i}{g(\omega_{ke})} \sum_c V_{ke,c} G_{cc}(\omega_{ke}) V_{c,ke} \right] \\
&= \lim_{x\to\infty} \frac{1}{\sqrt{L}} e^{ikx} |e\rangle \left[1 + a_e + a_o \right]
\end{aligned} \tag{4.15}$$

where the contour of the integral encompasses the upper k' plane, $|e\rangle$ is the mode profile in the y direction. the scattering amplitudues due to even and odd modes are defined as

$$\begin{aligned}
a_c &= -\frac{i}{g(\omega_{ke})} V_{ke,c} G_{cc}(\omega_{ke}) V_{c,ke} \\
&= -\frac{i\gamma_c}{\omega_{ke} - \widetilde{\omega_c} + i\gamma_c}
\end{aligned} \tag{4.16}$$

Similarly, the backward scattering is given by

$$\langle x=-\infty|T|ke\rangle = \frac{1}{2\pi}\int dk' \frac{1}{\sqrt{L}} e^{ik'x}|e\rangle \frac{\sum\limits_c V_{k'e,c} G_{cc}(\omega_{ke}) V_{c,ke}}{\omega_{ke}-\omega_{k'e}+i\epsilon}$$

$$= \lim_{x\to\infty} -\frac{i}{\sqrt{L}} e^{-ikx}|e\rangle \sum_c V_{-ke,c} G_{cc}(\omega_{ke}) V_{c,ke} \tag{4.17}$$

$$= \lim_{x\to\infty} \frac{1}{\sqrt{L}} e^{-ikx}|e\rangle (a_e - a_o) \tag{4.18}$$

where the contour of the integral encompasses the lower k' plane.

Now one readily verifies that the forward and backward scattering wave for the initial beam $|k\rangle$ is given by

$$\langle x=\infty|T|k\rangle = \frac{1}{2}\left[(2+a_e+a_o)\langle x=\infty|k\rangle + (a_e+a_o)\langle x=\infty|\overline{k}\rangle\right] \tag{4.19}$$

$$\langle x=-\infty|T|k\rangle = \frac{a_e-a_o}{\sqrt{2}}\left[\langle x=-\infty|-k\rangle + \langle x=-\infty|-\overline{k}\rangle\right] \tag{4.20}$$

Therefore, the following amplitude of the outgoing wave is obvious

$$\text{Forward transmission: } 1+\frac{a_e+a_o}{2}$$

$$\text{Forward transfer: } \frac{a_e+a_o}{2}$$

$$\text{Backward transmission: } \frac{a_e-a_o}{2}$$

$$\text{Backward transfer: } \frac{a_e-a_o}{2}$$

As shown by Fan *et. al.* [8], it is possible to force an accidental degeneracy between the even and odd modes, i.e. $\widetilde{\omega}_e = \widetilde{\omega}_o$. At resonance $\omega_{ke} = \widetilde{\omega}_e = \widetilde{\omega}_o$, then $a_e = a_o = -1$. Except for the forward transfer, the amplitudes of all the other outgoing waves vanish, 100% channel drop transfer is accomplished.

For the case of a beam injected into the lower waveguide, the amplitude of the outgoing waves are exactly the same as those in the upper waveguide case.

If the symmetrized localized states are odd in y direction, then a similar analysis applies and the same results are recovered except that the subscripts e and o are exchanged in the outgoing wave amplitude.

D. Four-Cavity Filter: Flat-top Transfer Function

For the system with four localized states as shown in Fig. 10, one advantage is the transfer function of the channel drop system can be improved. Generally, flat-top and sharp edges are the preferred form of the transfer function.

Assume the four states represented by $|\delta_x\delta_y\rangle$ have the symmetry δ_x and δ_y with respect to the mirror planes normal to x and y axes, respectively. Here, δ_x and δ_y take values e and o, which indicates even and odd states, respectively.

For such a system, both the $|ke\rangle$ and $|ko\rangle$ waves are scattered by the resonator system. Now the self-energy is given by

$$\Sigma_{\delta'_x\delta'_y,\delta_x\delta_y} = \frac{1}{L}\sum_{q,\delta''_y} \frac{V_{\delta'_x\delta'_y,q\delta''_y} V_{q\delta''_y,\delta'_x,\delta'_y}}{\omega - \omega_{q\delta''_y} + i\epsilon}. \tag{4.21}$$

Because $V_{\delta'_x\delta'_y,q\delta''_y} = V_{\delta'_x\delta'_y,q\delta'_y}\delta_{\delta'_y,\delta''_y}$, we have $\Sigma_{\delta'_x\delta'_y,\delta_x\delta_y} = \Sigma_{\delta'_x\delta_y,\delta_x\delta_y}\delta_{\delta_y,\delta'_y}$. By changing the sum over q to over $-q$ one easily shows the self-energy is also diagonal with respect to δ_x subspace. Therefore, the self-energy has the form

$$\Sigma_{\delta'_x\delta'_y,\delta_x\delta_y} = \frac{1}{L}\sum_{q} \frac{V_{\delta_x\delta_y,q\delta_y} V_{q\delta_y,\delta_x,\delta_y}}{\omega - \omega_{q\delta_y} + i\epsilon}\delta_{\delta'_x\delta'_y,\delta_x\delta_y}. \tag{4.22}$$

The forward transmission for the $|k\delta_y\rangle$ states is

$$\begin{aligned}
\langle x=\infty|T|k\delta_y\rangle &= \sum_{k'\delta'_y}\langle x=\infty|k',\delta'_y\rangle\langle k'\delta'_y|T|k\delta_y\rangle \\
&= \lim_{x\to\infty}\frac{L}{2\pi}\int dk'|\delta_y\rangle\frac{1}{\sqrt{L}}e^{ik'x}\left[\delta_{k'k} + \frac{1}{L}\frac{\sum\limits_c V_{k'\delta_y,\delta_x\delta_y}G_{\delta_x\delta_y}V_{\delta_x\delta_y,k\delta_y}}{\omega_{k\delta_y} - \omega_{k'\delta_y} + i\epsilon}\right] \\
&= \lim_{x\to\infty}\frac{1}{\sqrt{L}}e^{ikx}|\delta_y\rangle\left[1 - \frac{i}{g(\omega_{k\delta_y})}\sum_{\delta_x} V_{k\delta_y,\delta_x\delta_y}G_{\delta_x\delta_y}(\omega_{k\delta_y})V_{\delta_x\delta_y,k\delta_y}\right] \\
&= \lim_{x\to\infty}\frac{1}{\sqrt{L}}e^{ikx}|e\rangle\left[1 + a_{e,\delta_y} + a_{o,\delta_y}\right]
\end{aligned} \tag{4.23}$$

where the scattering amplitude due to the state $|\delta_x\delta_y\rangle$ is

$$\begin{aligned}
a_{\delta_x\delta_y} &= -\frac{i}{g(\omega_{k\delta_y})}V_{k\delta_y,\delta_x\delta_y}G_{\delta_x\delta_y c}(\omega_{k\delta_y})V_{\delta_x\delta_y,k\delta_y} \\
&= -\frac{i\gamma_{\delta_x\delta_y}}{\omega_{k\delta_y} - \widetilde{\omega}_{\delta_x\delta_y} + i\gamma_{\delta_x\delta_y}}
\end{aligned} \tag{4.24}$$

and the renormalized frequency and the linewidth of the localized states are given by

$$\widetilde{\omega}_{\delta_x\delta_y}(\omega)= \omega_{\delta_x\delta_y} + \frac{\mathcal{P}}{2\pi}\int dq \frac{|V_{\delta_x\delta_y,q\delta_y}|^2}{\omega-\omega_{\delta_x\delta_y}} \tag{4.25}$$

$$\gamma_{\delta_x\delta_y}(\omega)= \frac{1}{g(\omega)}|V_{\delta_x\delta_y,q\delta_y}|^2 \tag{4.26}$$

Similarly, one readily verifies that the reflected wave is

$$\langle x=-\infty|T|k\delta_y\rangle = \lim_{x\to\infty}\frac{1}{\sqrt{L}}e^{-ikx}|e\rangle\left[a_{e,\delta_y}-a_{o,\delta_y}\right] \tag{4.27}$$

Accordingly, for the injected beam $|k\rangle$ in the upper waveguide, the outgoing waves have the amplitudes

$$\begin{aligned}
\text{Forward transmission: } & 1+\frac{1}{2}(a_{ee}+a_{oe}+a_{eo}+a_{oo}) \\
\text{Forward transfer: } & \frac{1}{2}(a_{ee}+a_{oe}-a_{eo}-a_{oo}) \\
\text{Backward transmission: } & \frac{1}{2}(a_{ee}-a_{oe}+a_{eo}-a_{oo}) \\
\text{Backward transfer: } & \frac{1}{2}(a_{ee}-a_{oe}-a_{eo}+a_{oo})
\end{aligned}$$

If we neglect the difference between $|ke\rangle$ and $|ko\rangle$ modes, they reduce to the case investigated by Fan *et. al.*. It can be shown that one can force the following conditions

$$\widetilde{\omega}_{ee}=\widetilde{\omega}_{oe},\ \widetilde{\omega}_{eo}=\widetilde{\omega}_{oo} \tag{4.28a}$$

$$\gamma_{ee}=\gamma_{oe}=\gamma_{eo}=\gamma_{oo}\equiv\gamma \tag{4.28b}$$

$$\widetilde{\omega}_{ee}-\widetilde{\omega}_{oo}=2\gamma \tag{4.28c}$$

Then the forward transmission is given by

$$\frac{(\omega-\omega_0)^4}{(\omega-\omega_0)^4+4\gamma^4} \tag{4.29}$$

where $\omega_0=\frac{1}{2}(\widetilde{\omega}_{ee}+\widetilde{\omega}_{oo})$ and the forward transfer is given by

$$\frac{4\gamma^4}{(\omega-\omega_0)^4+4\gamma^4} \tag{4.30}$$

which has the form of "maximum-flat" function, as shown in Fig. 11 .

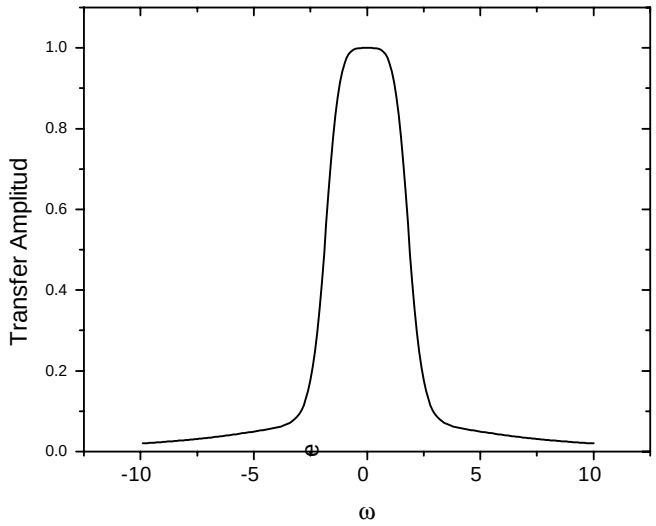

Fig. 11

The backward reflection and backward transfer waves both vanish. However, one should bear in mind that these formulae are only approximately correct near the region of resonance. Because, generally speaking, the renormalized resonance frequency and the linewidth of the localized states are functions of $\omega_{k\delta_y}$, the frequency of the propagating states interacting with this localized states. This is testified by the difference in the intensity profile (or the actual linewidth) between $|ee\rangle$ and $|oe\rangle$, or $|eo\rangle$ and $|oo\rangle$ states.[8] Note this difference also exists in the case of two localized states. However, in the case of two localized states, this doesn't affect the 100% transmission at the resonance because by forcing the degeneracy of the even and odd localized modes at resonance only, the contribution from these two modes are exactly the same at the resonance. Even we introduce the coupling between the propagating states, this is still true because the odd propagating states are not scattered, we need to force the degeneracy at one frequency, i.e. ω_{ke}.

We note that to allow the transfer function to have approximately the maximum flat form represented by Eq. (4.30), the renormalized frequency and linewidth should not change much when ω_{ke} varies from $\omega_0 - \gamma$ to $\omega_0 + \gamma$. One possible solution is to chose the frequency range where these quantities are not sensitive to the frequency of the propagating states. This

requires that the interaction coefficients $V_{k\delta_y,c}$ are not sensitive to the wavevector k. As shown in the first part of the report, the electric field profile in the crystal is mainly the unperturbed states at the band extreme, with a small perturbation of the order k. Then the interaction coefficient

$$V_{k\delta_y,c} = \int E_{k\delta_y} V(r) E_c d^2 r \tag{4.31}$$

is not sensitive to k. In this range, one can treat the equations Eq. (4.28) as identities when the frequency varies. Then the maximum flat function is quite an exact approximation of the transfer function.

E. High Order Flat-top Transfer Function

Fan *et. al.* explored the possibility of generating higher order flat top functions by increasing the number of localized states. But as the number localized states increases, they had to assume the coupling V_{kc} involves only the four localized states centered nearest the two waveguides. They also neglected the coupling V_{c_1,c_2} between most of localized states. Even with such simplification, they were not able to give a higher order flat top function finally.

The theoretic analysis based on symmetry given above cast a new light on this problem. From the point view of group theory, it is the orthogonality of different symmetric states that results in the decoupling of localized states. Each decoupled localized state is an eigenstate of the complete set of commuting operators(CSCO) of the symmetry group of the Hamiltonian. And due to symmetry, the propagating modes couple only those localized modes with the same symmetry with them. The symmetry naturally diagonalizes the Hamiltonian in the reduced space of localized states. From above analysis, one finds that enhancing the symmetry of system will give more coupling terms, which generate high order flattop transfer function.

As an example, we will discuss the case where we have 3-fold symmetry. The sketch of the system is shown in Fig. 12.

The crystal itself is a triangular lattice. It is important to notice one needs to increase the number of waveguides in addition to increasing the number of cavities. The symmetry of the waveguides must be the same as that the cavities otherwise the coupling will be restrict to the common subgroup of the symmetry group of the waveguides and that of the cavities. In this case, if we still have two waveguides, the common subgroup only contains the mirror normal to the waveguides, which will not give any useful transfer coupling.

As in the case of two waveguides, we need to maintain two cavities by the side of each

waveguide for suppression of backward scattering. We can force the occidental degeneracy(as Fan *et. al.* did in the two waveguide, by properly setting the parameters of the cavities and its surrounding cells) for the two symmetrized states, which are even and odd with respect to the mirror plane normal to each waveguide. Then the backward scattering is suppressed in each waveguide.

Let the states in waveguide 1, 2, and 3 be $|k\rangle$, $|k'\rangle$, and $|k''\rangle$, respectively. In our notation, these three states all have the same wavevector k, but they are in different waveguides. If total area of the 3 guided region is much less than the system area, then one readily finds that the longitudinal wavevector in each waveguide is a good quantum number by showing the overlap integral between modes with different wavevectors vanishes as system area goes to infinity (particularly, one should assume the crystal region encompassed by the three waveguides goes to infinity with the same rate as the system, but the width of the waveguides stays as a constant). In practice, all these actually mean the system area and the area encompassed by the waveguides should be much larger the total area of the three waveguides. This is not difficult to achieve. Here, we assume the cavities have areas even smaller than the guides, therefore, their correction to the integral between different k states can be completely neglected. But they definitely contribute to the overlap integral between propagating modes and localized modes because the localized modes have amplitude of order unity in the cavities. while the propagating modes have amplitude approaching zero everywhere while system area goes to infinity. The eigenstates of the rotation operator C_3 are

$$|k,1\rangle = \frac{1}{\sqrt{3}}(|k\rangle + |k'\rangle + |k''\rangle) \tag{4.32}$$

$$|k,\delta\rangle = \frac{1}{\sqrt{3}}(|k\rangle + \delta|k'\rangle + \delta^2|k''\rangle) \tag{4.33}$$

$$|k,\delta^2\rangle = \frac{1}{\sqrt{3}}(|k\rangle + \delta^2|k'\rangle + \delta|k''\rangle) \tag{4.34}$$

$$\tag{4.35}$$

which have eigenvalues 1, δ, δ^2, correspondingly, and $\delta = e^{\frac{i2\pi}{3}}$. The localized states can also

be symmetrized, similarly. In this case, the six symmetrized states are

$$
\begin{aligned}
|1e\rangle &= \frac{1}{\sqrt{6}}\left[|11\rangle + |12\rangle + (|21\rangle + |22\rangle) + (|31\rangle + |32\rangle)\right] \\
|1o\rangle &= \frac{1}{\sqrt{6}}\left[|11\rangle - |12\rangle + (|21\rangle - |22\rangle) + (|31\rangle - |32\rangle)\right] \\
|\delta e\rangle &= \frac{1}{\sqrt{6}}\left[|11\rangle + |12\rangle + \delta\left(|21\rangle + |22\rangle\right) + \delta^2\left(|31\rangle + |32\rangle\right)\right] \\
|\delta o\rangle &= \frac{1}{\sqrt{6}}\left[|11\rangle - |12\rangle + \delta\left(|21\rangle - |22\rangle\right) + \delta^2\left(|31\rangle - |32\rangle\right)\right] \\
|\delta^2 e\rangle &= \frac{1}{\sqrt{3}}\left[|11\rangle + |12\rangle + \delta^2\left(|21\rangle + |22\rangle\right)\delta\left(|31\rangle + |32\rangle\right)\right] \\
|\delta^2 o\rangle &= \frac{1}{\sqrt{3}}\left[|11\rangle - |12\rangle + \delta^2\left(|21\rangle - |22\rangle\right) + \delta\left(|31\rangle - |32\rangle\right)\right]
\end{aligned}
\tag{4.36}
$$

Due to the orthogonality of symmetrized states, there is no coupling between these symmetrized localized states. And the coupling between the propagating states and the localized states is restricted to those states having the same eigenvalues of C_3.

A calculation similar to that given for the case of 2-fold symmetry shows for an beam e^{ikx} injected into waveguide 1, the scattering amplitudes are

$$
\begin{aligned}
\text{Forward transmission: } & 1 + \frac{1}{3}(a_{1e} + a_{1o} + a_{\delta e} + a_{\delta o} + a_{\delta^2 e} + a_{\delta^2 o}) \\
\text{Forward transfer in waveguide 2: } & \frac{1}{3}[a_{1e} + a_{1o} + \delta^2(a_{\delta e} + a_{\delta o}) + \delta(a_{\delta^2 e} + a_{\delta^2 o})] \\
\text{Forward transfer in waveguide 3: } & \frac{1}{3}[a_{1e} + a_{1o} + \delta(a_{\delta e} + a_{\delta o}) + \delta^2(a_{\delta^2 e} + a_{\delta^2 o})] \\
\text{Backward scattering: } & \frac{1}{3}(a_{1e} - a_{1o} + a_{\delta e} - a_{\delta o} + a_{\delta^2 e} - a_{\delta^2 o}) \\
\text{Backward transfer in waveguide 2: } & \frac{1}{3}[a_{1e} - a_{1o} + \delta^2(a_{\delta e} - a_{\delta o}) + \delta(a_{\delta^2 e} + a_{\delta^2 o})] \\
\text{Backward transfer in waveguide 3: } & \frac{1}{3}[a_{1e} - a_{1o} + \delta(a_{\delta e} - a_{\delta o}) + \delta^2(a_{\delta^2 e} - a_{\delta^2 o})]
\end{aligned}
\tag{4.37}
$$

where $a_{\delta_3,\delta_x} = -\frac{i\gamma_{\delta_3,\delta_x}}{\omega_{k,\delta_3} - \omega_{\delta_3,\delta_x} + i\gamma_{\delta_3,\delta_x}}$, $\delta_3 = 1,\ \delta,\ \delta^2$, and $\delta_x = e,\ o$. Forcing $\omega_{\delta_3,e} = \omega_{\delta_3,o}$ and $\gamma_{\delta_3,e} = \gamma_{\delta_3,o}$, one finds that the backward scatterings in all 3 waveguides vanish. The even and odd terms in forward scatterings are the same, so they add up and give a factor of two.

Because there is no difference between even and odd terms, then we neglect from now on the subscripts e and o. We find that if we choose

$$
\gamma_\delta = \gamma_{\delta^2} = b\gamma_1 \tag{4.38}
$$

$$\omega_\delta - \omega_1 = -(\omega_{\delta^2} - \omega_1) = \sqrt{3}\gamma_\delta \tag{4.39}$$

where b is an arbitrary real number, then at the frequency ω_1 unitary transfer to waveguide 2 will be realized. For convenience, let's use the normalized frequency $\Omega = (\omega - \omega_1)/\gamma_\delta$ Lengthy calculations show the forward transmission and forward transfer in waveguide 2 are given by

$$\text{Forward transmission: } \frac{(4b+1)^2\Omega^4 + (b\Omega)^2(3\Omega^2-10)^2}{9(1+b^2\Omega^2)(\Omega^4-4\Omega^2+16)} \tag{4.40}$$

$$\text{Forward transfer in waveguide 2: } \frac{4}{9}\frac{[6+(b-1)\Omega^2]^2 + \Omega^2(1+2b)^2}{(1+b^2\Omega^2)(\Omega^4-4\Omega^2+16)} \tag{4.41}$$

By adjusting the value of b, we can get better flat top function than in the case of four localized states. In Fig. 13 and 14, we draw the comparison, the optimum value for b is about 0.3. Larger values of b will result in sharp peaks, whereas smaller b will generate sidelobes.

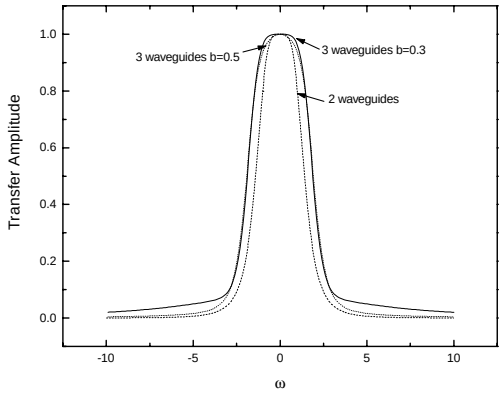

Fig. 13

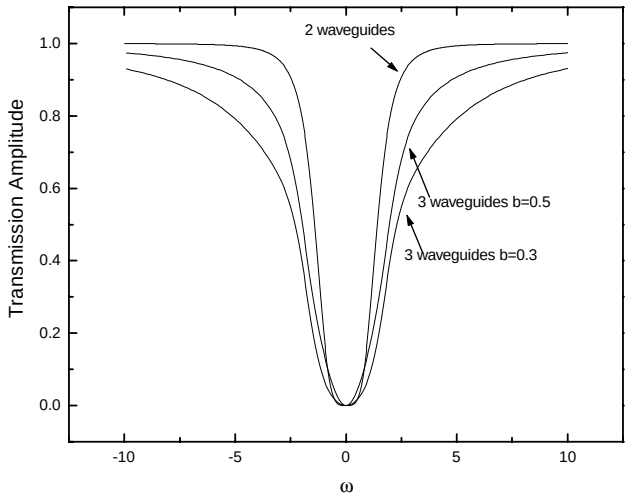

Fig. 14

The advantage of this system is obvious, we had an additional parameter to control the lineshape of the transfer function. Further numerical study is needed to find how to choose parameters of the cavities to realize this system.

It is not difficult to extend above argument to a 4-fold system, where we can still use a square lattice. But there should be 4 waveguides intersecting along the edges of a square and there should be a total of eight localized states. The transfer function will be of higher order. The denominator will be of eighth power in frequency.

V. LOCALIZATION TRILOGY AND THE C-NUMBER

A. Introduction

Recent years have witnessed a consistent interest in Photonic Band Structure [25]. Two themes are present in this field of research. The potential for applications to various devices, e.g. high efficiency laser[3] and antenna[26] has attracted most experimental researchers' attention, while impetus from the theoretical side lies in its candidacy for an ideal structure to test the theory of localization[15].

Following the pioneering steps of P. W. Anderson[9] and N. F.Mott[10], numerous researchers have devoted the study and observation to the electron localization in disordered solids. Some general features of localization are well estabished now[11]. However, due to the existence of electron-electron interaction and electron-phonon interaction, theoretical predictions often meet with difficulties in accounting for the experimental data definitively. S. John first explored the possibility of observing localized states of light in a dielectric medium[2], in which the complication of the interactions associated with electrons are avoid so the further study of localization[12] in such systems is facilitated. Experiments quickly verified the existence of weak localization in the form of coherent backscattering [13]. However, for the implementation of strong localization of light, there is another serious problem: the effective energy of the wave equation of light in an inhomogeneous medium is always positive, and even worse, the energy of the photons is always higher than the potential barriers[14]! After Yablonovitch first proposed a three-dimensional dielectric structure with Photonic Band Gaps (PBG), John recognized[15] that a moderate disordered perturbation of this structure may provide the key to the predictable and systematic observation of strong localization of light. The gist of his theory is that the underlying superlattice provides a band gap for the frequency range of localization because of the remnant geometric Bragg resonances. Though studies along this theoretical line [16, 18, 17] have been carried out by several groups, some fundamental questions have remained unsolved as discussed be-

low. Many studies (experimental and theoretical) have been conducted on the disorder in a homogeneous background[19, 20], instead of in a superlattice. Their results can not be generalized to localization in PBG materials because of the absence of Bragg scattering in the homogeneous background. Therefore the problem of strong localization in moderately disordered lattice is far from fully understood. For example, the only known embodiment of the "interplay between order and disorder"[15] is that the localization is present at moderate, rather than at high degree of disorder, but will this interplay bring some other drastic changes to the whole picture of localization? Further, John has argued that the localization mechanism due to the remnant geometric Bragg resonances in dielectric structure is a new one[15]. Then the question remains whether the localization mechanism with which we are familiar in Anderson model is also present in a dielectric structure? If it is, how will these two mechanisms interact with each other, and what will there be interesting the coexistence of these two mechanisms will bring?

We are not well equipped to answer these questions. The analytic treatment has proved to be difficult. The well established formalism[27] assumes a low concentration of scatterers or a low degree of disorder. However, as we shall see, the most interesting localization behaviors in PBG materials occur at moderate disorder. On the numerical side, calculations with dimensions higher than one usually require prohibitive time and/or memory. So it is not surprising that these questions still reside in the category of the unsolved. Even John's original proposal(strongly localized states present at moderate disorder) has not been directly verified by numerical calculation.

However, R. D. Meade *et. al.* [28] have introduced a memory-economical computing scheme in their calculations of photonic bands and impurity energy levels. This method has greatly enlarged the size of systems that we are able to calculate. But, applied to the supercell problem, this algorithm usually needs to calculate all the states with frequencies lower than the desired one, a requirement of orthogonalization. As the supercell grows larger and larger, the workload becomes intolerable. In this chapter, a new scheme for the supercell problem is developed to calculate a few eigenstates with frequencies closest to a

specific value without the need to calculate of the lower states.

With this method, we directly show by field pattern that, at moderate disorder, there exist strongly localized states inside the original photonic band gaps. We find that as the degree of disorder increases, the states in or near the PBG first localize, then delocalize, finally localize again. This localization trilogy is clearly shown due to the cooperation of two localization mechanisms, which are distinguished by their different ranges of coherence. Due to their different sensitivies to these two localization mechanism, the TM and TE modes exhibit different localization behaviors. Our analysis answers, simultaneously, the problems proposed at the end of the second paragraph.

The partition number[29] commonly used proves to be a very useful measure to analyze wavefuntions in localization problems. However, sometimes it does not contain all the desired information. To study the nature of localization centers at different frequencies, a new measure, the C-number, is introduced in our study. A sum rule involving the C-number and partition number is obtained in this work. With the C-number,, we find that the sites a photon prefers to occupy are obviously related to frequency. The frequency distribution of localization centers established at moderate disorder is maintained till strong disorder, except in the frequency ranges around the original gaps.

The structure of this chapter is as follows. In section II, the problem and the computational scheme are described. In section III, we introduce the C-number and propose a sum rule involving the C-number and partition number. In section IV, first, we show the localization process plays a trilogy as the degree of disorder varies and discuss the underlying mechanism, then the distribution of C-numbers with frequency is studied. Section V contains the conclusion.

B. Computational Scheme

In the photonic crystal, the dielectric constant $\epsilon(\mathbf{r})$ is a function of position. The electromagnetic field is determined by the solution of the Maxwell's equations. For the reason

of continuity of the field vectors, it is convenient to solve these equations in terms of the magnetic field vector $\mathbf{H}(\mathbf{r})$. The wave equation is then

$$\nabla \times [\frac{1}{\epsilon(\mathbf{r})} \nabla \times \mathbf{H}(\mathbf{r})] = (\frac{\omega}{c})^2 \mathbf{H}(\mathbf{r}) \tag{5.1}$$

with the transverse field condition $\nabla \cdot \mathbf{H}(\mathbf{r}) = 0$. A typical two-dimensional dielectric superlattice is either a periodic array of dielectric columns in the air or a periodic array of air columns in the dielectric bulk. The centers of the columns can be arranged into any type of two-dimensional lattice. The lattice studied in this chapter is a triangular lattice of dielectric columns in the air. There are two parameters in the definition of this periodic dielectric structure, the dielectric constant of the dielectric material and the column radius. In this study, the dielectric constant is chosen to be $\epsilon_a = 13$, which is close to the value of gallium arsenide. The column radius is $0.32a$, where a is the lattice constant. For disordered systems, the supercell comprises 256 (16×16) unit cells and we calculate up to 16400 plane waves for each polarization. The relative deviation of column dielectric constants ϵ is uniformly distributed in the range $-W/2 < \epsilon/\epsilon_a - 1 < W/2$, where W indicates the degree of disorder.

Meade *et. al.* first introduced an optimization algorithm for the calculation of photonic band structure[28]. The optimization algorithm greatly reduces the required memory because it changes the wavefuntions each step instead of changing the operators. Hence the operator need not be stored as it can be constructed impromptu at a reasonable expense of time by using the Fast Fourier Transform(FFT). Still, when applied to the supercell problem, the workload of any optimization algorithm is overwhelming because the states we are interested in are usually inside or near the gap. The orthogonalization process of the algorithm requires us to calculate all the states lower than the target state; therefore one must calculate an entire band of states!

We have developed a method which enables us to calculate several states closest to a specific energy without calculating lower energy states. Suppose the energy functional to be $\Psi^+ Q \Psi$, Q is the main operator, Ψ is the wavefunction. If the optimization object is

$\Psi^+(Q-E)^2\Psi$ (E is the specified energy) rather than the energy functional, the eigenstates obtained first are those with energies nearest to E. We note the operator $(Q-E)^2$ can also be constructed impromptu with FFT algorithm, therefore this method leaves intact all the time and memory saving features of the previous algorithm. With this method, we have performed a systematic calculation of localization of electromagnetic waves in two-dimensional structures. For every frequency studied, five states nearest to this frequency are calculated for TM (with the magnetic field vector lying in plane) and TE (with the magnetic field vector normal to the plane) modes respectively. Then for each state, we define the coarse-grained field $\widetilde{H}(i,j)$ by integrating the square modula of the magnetic field in each unit cell Ω_{ij}

$$\widetilde{H}^2(i,j) = \int_{\Omega_{ij}} |\mathbf{H}(\mathbf{r})|^2 \mathbf{dr} \tag{5.2}$$

These coarse-grained spatial field patterns are recorded on the hard disk to save space.

C. A New Measure: C-number

The partition number introduced by P. Dean[29] is a powerful tool to analyze the large volume of data obtained from the *ab initio* calculation. The partition number is defined by

$$P = \left[\sum_i |\Psi_i|^4\right]^{-1} \tag{5.3}$$

where Ψ_i is the normalized wavefunction. It roughly gives the number of sites where the mode is significantly excited. Thus $1/P$ indicates the degree of localization of a state. However, often one needs to obtain more information about the character of the microscopic states than given solely by the partition number. For the localization problem, one character we are interested in is the nature of the localization center(s) of a localized state. From the partition number one may at best get a feeling how fast the wavefunction decays from these centers. But to find which kind of sites are preferred centers for a specific state, one needs another measure.

A close inspection of the spatial dielectric distribution and the field patterns of several localized states reveals the meaning of the new measure to be introduced.

Figure 15 (a) presents the distribution of the cell-average dielectric constants in 16×16 unit cells(for visual ease, the triangular lattice is drawn as a square one).

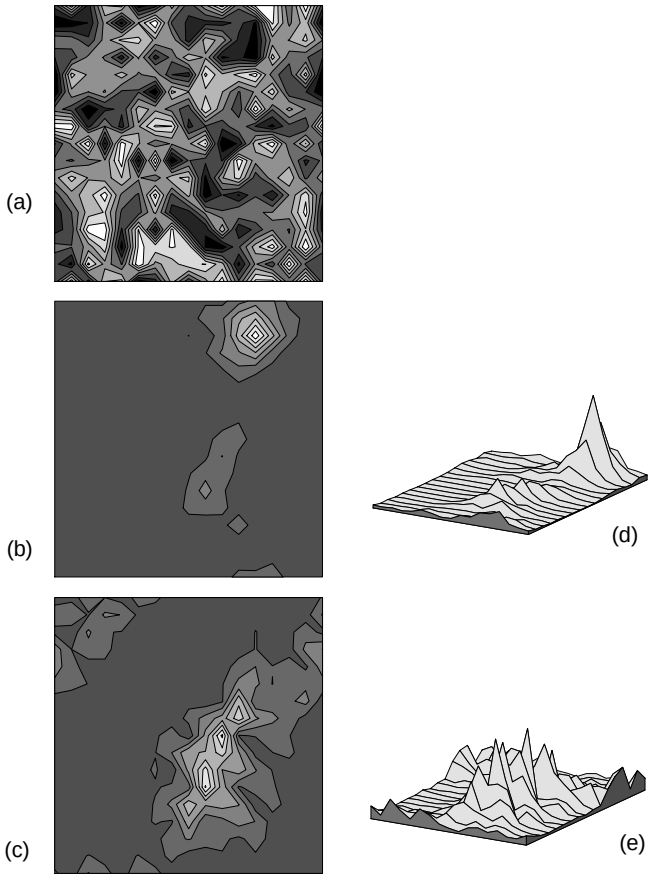

Fig. 15

In the gray scale contour maps, the white color indicates the highest value, whereas the black color, the lowest. We use the contour map because it best visualizes the relation between the average dielectric constant distribution and the localization centers. However, one should keep in mind that the actual average dielectric constant distribution is defined on a 16×16 discrete grid. In figure 15 (b) and (d), a strongly localized TM state is drawn in two ways against the map of the dielectric constant distribution. This state is found for the strength of disorder $W = 1.0$, at the frequency $\frac{\omega a}{2\pi c} = 0.228$, (subsequently, all frequencies

are given in the unit of $\frac{2\pi c}{a}$ in this chapter); with a partition number 11.7. Note that for the periodic system with our division of unit cells, the first gap of the TM mode ranges from 0.209 to 0.273, and the first TE gap is between 0.325 and 0.360. The localization center of this state corresponds to the low dielectric island near the upper edge, as one sees by comparing Fig. 15 (a) and (b). The TE state shown in Fig. 15 (c) and (e) is found for $W = 0.4$, at the frequency 0.331, with a partition number 32.9. Clearly, it is localized around a chain of low dielectric constant islands in the middle of the system. However, for less localized states, the field patterns are not so simple as Fig. 15 (b) and (c), and the correspondence between the field patterns and the dielectric distribution is not easy to detect by direct inspection. In most cases, one needs to introduce the C-number defined below to measure this correspondence.

Suppose we have a coarse-grained magnetic field $\widetilde{H}(i,j)$ defined on the lattice level(so i, j run all over lattice sites). The C-number is defined by

$$C = \rho(\epsilon, \widetilde{H}^2) \tag{5.4}$$

where $\epsilon(i,j)$ is the average dielectric constant in the unit cell Ω_{ij} and the correlation coefficient $\rho(X,Y)$ between two random variables $X(i,j),\ Y(i,j)$ defined on lattice sites is given by the well-known equations

$$\begin{aligned} \rho(X,Y) &= \frac{cov(X,Y)}{\sigma_X \cdot \sigma_Y} \\ cov(X,Y) &= \frac{1}{N-1}\sum_{i,j}(X(i,j)-\overline{X})(Y(i,j)-\overline{Y}) \\ \sigma_X &= \sqrt{cov(X,X)} \end{aligned} \tag{5.5}$$

where N is the total number of sites, and $\overline{X}$ and $\overline{Y}$ are the mean values of X and Y on the lattice. For the TM state given in Fig. 15 (b) and (d), the C-number is -0.170. This negative C-number indicates the coarse-grained field has a large amplitude around some cells containing columns with low dielectric constants. The C-number for the TE mode shown in Fig. 15 (d) and (e) is -0.224.According to the location of their frequencies in the gap,

these two states may be called acceptor-like states.[30] This kind of states are associated with negative C-numbers.

A sum rule can be obtained for the C-number and the partition number. When the disorder is not very strong, a large part of the original gap survives. Then the single band approximation holds(as assumed in Anderson model), which means that a mode in a certain band of the disordered system is a linear combination of states in the corresponding band of the periodic system. This implies,

$$\sum_n \psi_n^+(\mathbf{r})\psi_n(\mathbf{r}') = \sum_k \phi_k^+(\mathbf{r})\phi_k(\mathbf{r}') \tag{5.6}$$

where $\phi_k(\mathbf{r})$ and $\psi_n(\mathbf{r})$ are the states of periodic and disordered systems, respectively; the summations of k and n extend over a single band in the corresponding systems. Let $\mathbf{r} = \mathbf{r}'$, and integrate the right hand side in any unit cell, one finds that the integral is a constant, m(m is a positive integer), independent of the position of the cell. For our coarse-grained field in the disordered system this means

$$\sum_n \widetilde{H}_n^2(i,j) = m \tag{5.7}$$

Another useful equation is

$$\sigma^2_{\widetilde{H}^2} = \frac{1}{N-1}(\frac{1}{P} - \frac{1}{N}) \tag{5.8}$$

Now one readily proves:

$$\begin{aligned}\sum_n C_n \cdot \sqrt{\frac{1}{P_n} - \frac{1}{N}} &= \frac{\sqrt{N-1}}{\sigma_\epsilon}\sum_{i,j}(\epsilon(i,j) - \overline{\epsilon})\sum_n \widetilde{H}_n^2(i,j) \\ &= 0\end{aligned} \tag{5.9}$$

where C_n and P_n are the C-number and partition number corresponding to $\widetilde{H}_n(i,j)$. In terms of energy spectrum, we have

$$\int \rho(E)C(E)\sqrt{\frac{1}{P(E)} - \frac{1}{N}}dE = 0 \tag{5.10}$$

Several points should be noted for this sum(or integral). First, fully extended states don't contribute to this sum. Second, for the strongly localized states, the C-numbers may be

quite small(compared with fairly localized states), however, their small partition numbers compensate for it so that their contribution to the sum is still considerable. Due to the enormous time required for calculation of an entire band of states, we only perform a rough check of the sum rule on a 8×8 lattice. For $W = 0.2$, The sums in Eq. (9) divided by the correpsonding sums of absolute values are 0.07 and 0.18 for the TM mode and TE mode, respectively. When we increase the iteration times by one third, the above values reduce to 0.05 and 0.14. We also note a convergence of the above values from a 4×4 lattice to a 8×8 lattice. This sum rule will be better satisfied on a 16×16 lattice, where the ratio of a typical interband component to a typical intraband component in a perturb state is about 1% and 3% according to the energy difference denominators in the perturbation theory.

D. Results and Discussion

1. Localization Trilogy

At first, we study the localization behavior of the states near some specific frequencies as the degree of disorder changes. As shown in Fig. 15, very strongly localized states are found in the original gap at *moderate* disorder($W = 1.0$ for the TM mode, and $W = 0.4$ for the TE mode), as predicted by John[15].

The localization process of the states shows a complex feature. It is well-known that in the Anderson model, the states become more localized with increasing degree of disorder.[31] Recently, Freilikher *et. al.*[18] have found that for frequencies in the gap, there may exist an initial stage of enhancing transmission with increasing degree of disorder before the final stage of attenuating transmission at strong disorder. This has also been noted in a two-dimensional system, [17] though, for the range of disorder studied, the final attenuation range was not reached. The characteristic of this kind of enhancing transmission is that it occurs only in the gap and starts from infinitely weak disorder, hence it was attributed to the increasing of density of states(DOS) in the gap due to the presence of disorder.

However, question remains how the localization of microscopic states evolves with increasing disorder. Specifically, do the variation of localization lengths of the states have the features corresponding to the results of the studies of transmission? We find the localization of states shows more complex process than that reflected by studies of transmission, and this process is explained by the coexistence of two localization mechanism assoicated with different ranges of coherence.

Figure 16 presents the evolution of five states with frequencies slightly above the lower edge of the lowest gap for the TM ($\frac{\omega a}{2\pi c} = 0.212$) and the TE mode ($\frac{\omega a}{2\pi c} = 0.329$), respectively.

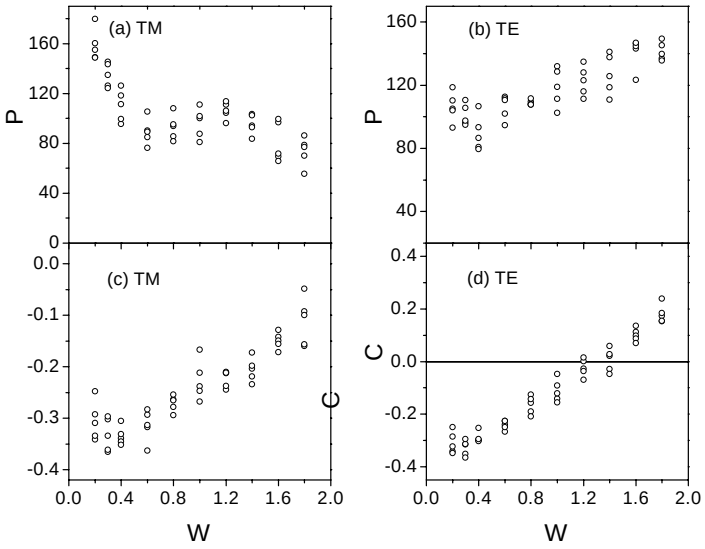

Fig. 16

It shows that the localization behavior, or more appropriately for this case, the localization-delocalization behavior of the TM mode can be described as a trilogy. When the degree of disorder W is less than 0.6, the localization of the states becomes more pronounced with increasing W. After that, the states begin to delocalize until W=1.2; then they show the localization trend again with a further increase in W. What we find is the delocalization of states begins at some intermediate disorder, and the delocalization is also found in the original band(as shown later), where DOS is generally decreasing. However, this surprising trilogy, can be well explained by considering the joint effect of two localization mechanisms.

When disorder is weak, the remnant Bragg resonant scattering of the underlying superlattice results in localization of photons. As the dielectric constants of the columns deviate farther and farther from the original value, the states presented in Fig. 16 localize around some low dielectric islands as those shown in Fig. 15. The difference between the dielectric constants of these islands and the average periodic background increases as W increases, so the localized states feel stronger Bragg scattering from the underlying superlattice, with the effect of further confining them around those islands. But when the disorder is very strong, the remnants of the underlying superlattice are completely destroyed. Then the localization process enters into another range. Whereas the localization mechanism provided by Bragg scattering is a long-range coherent effect, the localization in the strongly disordered system is of Anderson type, i.e., it is a local effect. The localization length is mainly determined by the local mismatch (the difference of dielectric constants between adjacent cells within several lattice constants), rather than by the deviation from the average background. But there must be a range of the degree of disorder where the Bragg scattering effect is diminishing while the Anderson localization is enhancing. The Anderson localization is not as strong as that produced by Bragg scattering, at least in this intermediate range of disorder; so the states begin to delocalize. John argued[15] that for weak disorder the wavelength entering the Ioffe-Regel[32] condition should be the inverse of the fluctuation in the wave vector from the Bragg plane; then we propose that for very strong disorder this wavelength should be the free-photon wavelength. For intermediate degrees of disorder, neither of these two lengths meets the Ioffe-Regel condition(in fact, the first length is not well defined for fairly strong disorder), so the states delocalize.

For the TE mode, Fig. 16 (b) shows that the localization-delocalization process ends in the second stage. The third stage will appear if one sets the average dielectric constant of the columns much larger, which provides greater local mismatch. There is a simple argument to explain why TE modes are resistant to the Anderson localization. The amplitudes of the band-edge TE modes are more concentrated in the air region and this is more obvious in a system formed by dielectric columns in air[33]. In the structure treated here, the air region is

connected through the entire system. From the viewpoint of percolation, this is unfavorable to localization, particularly to that of the Anderson type, because the percolation is a short free-path process, while the localization due to Bragg scattering depends on large-scale resonance. The different localization behavior of TM and TE modes thus reveals a major difference of the Bragg type localization mechanism from the Anderson type.

The C-numbers for this system are presented in Fig. 16 (c) and (d). Generally, in the inital localization stage ($W \leq 0.6$ for the TM mode, and $W \leq 0.4$ for the TE mode) the magnitudes of C-numbers increase, then remain nearly constant as the disorder increases. This is another proof to the effect of the Bragg scattering in this stage of localization: the states are becoming more localized around some low dielectric cells. However, there are many such cells in the system. As one state becomes more localized around only one, or several of them, the C-number of the state will suffer a decrease. But because the amplitude of the mode at the localization centers is greatly enhanced, this decrease is not significant. Furthermore, this slight decrease of the magnitudes of C-numbers at the end of the initial localization stage should not be confused with the obvious decrease in the delocalization stage, which is due to the diffusion of the mode amplitude into high dielectric constant cells. For the TE mode, the C-numbers finally become positive as a result of the "invasion" of upper band. The TE gap is much smaller than the TM gap, so it disappears(about W=0.9) very quickly as W increases. Then there is a mixing of the donor-like(associated with positive C-numbers) and acceptor-like states, the C-numbers tend to be neutral. In the end, the states of the upper band further move down, and crush onto the original lower band. These states (acceptor-like) maintain their positive C-numbers till very large W, as to be shown in the next subsection.

We also studied the states at another frequency slightly below the gap, $\frac{\omega a}{2\pi c} = 0.202$ for the TM mode and $\frac{\omega a}{2\pi c} = 0.319$ for the TE mode, as shown in Fig. 17.

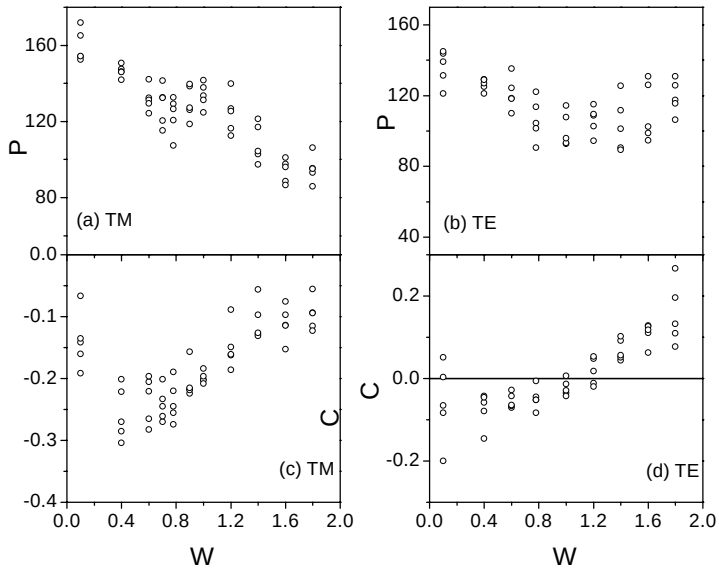

Fig. 17

The delocalization stage for TM mode is not as pronounced in Fig. 17 (a) as it is in Fig. 16 (a). This shows that the competition between the diminishing Bragg localization and the enhancing Anderson localization nearly reaches a balance in this frequency range. The delocalization is more obvious for the TE mode, which is due to the absence of the final localization stage, as in the gap. The graphs of C-numbers for this frequency are nearly the same as those for the frequency inside the gap. For the TE mode, some C-numbers are positive in this frequency range for very weak disorder. This is due to the distribution of C-numbers with frequency as discussed in the next subsection.

2. Frequency Distribution of C-numbers

In this subsubsection, we fix W and study the localization feature at different frequencies. In Fig. 18, W is set to 0.8, at this intermediate degree of disorder, the remnant gap for the TM mode is from 0.222 to 0.261, while for TE mode from 0.341 to 0.347. One sees that there is a considerable drop of partition number at the band edge. (Note: in Figs. 18 and 19, the axis breaks correspond to the remnant gaps, but in Fig. 20, they do not since there

is no remnant gap for both modes. The axis break in Fig. 20 is purely for change of scale in different frequency region)

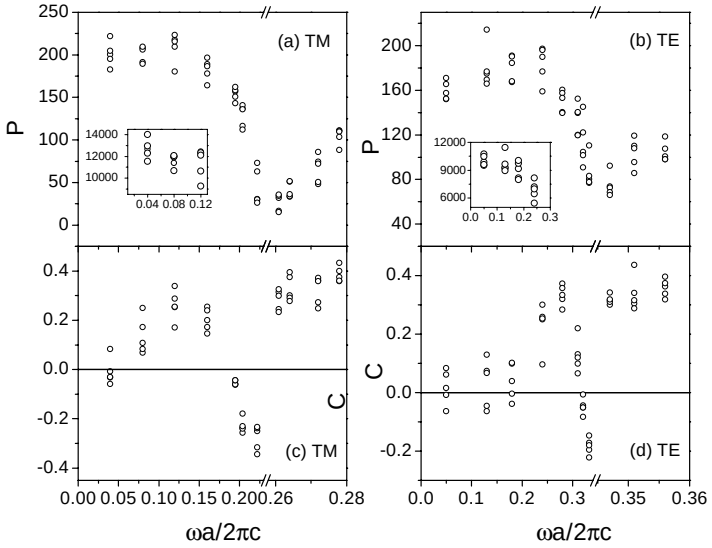

Fig. 18

It is well-known that the low frequency modes should be well extended, but there seems some slight drop of P in this range. To solve this problem, we calculated the partition number on the entire grid, so that the maximum P is about 16400. This kind of partition numbers are plotted in the insets of Fig. 18 (a) and (b). Clearly, these partition numbers increase consistently as frequency decreases. The difference between the partition number on the lattice basis and that on the grid basis is due to the inner structure of the field pattern. In fact, for most states in the lowest band, the partition number on the lattice basis is mainly determined by the localization of the wave on the lattice level, and the trend of two kinds of partition numbers is found to agree well. However, when the frequency approaches zero, the coarse-grained field is nearly uniform on the lattice level. Now the delocalization, or more properly, the redistribution of the wave amplitude occurs inside unit cells, particularly across the interfaces of the dielectric columns and the air region. But, generally, the localization problem is concerned with behavior on the lattice level(as in the Anderson model).

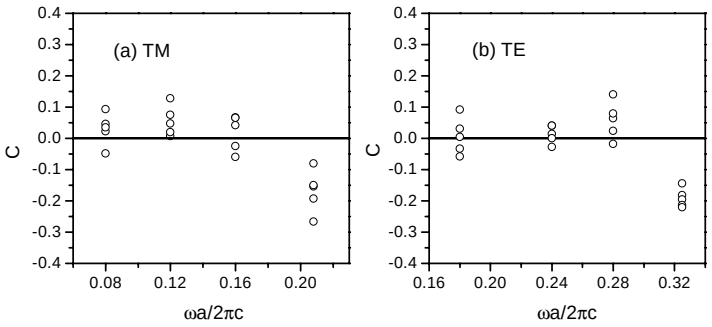

Fig. 19

The C-number distribution shows clearly the division between the donor-like and acceptor-like states by the gap. The donor-like states have positive C-numbers and the acceptor-like states have negative C-numbers. The discontinuity of the frequency distribution of the C-numbers occurs at the gap. In the band, the C-numbers vary continuously with frequency. This means the dielectric constants of the columns around which a state prefers to stay vary continuously with frequency. Deep in the lower band, the C-number is positive, as one expects from the sum rule. Physically, this is due to the balance of the local DOS. The sum of local DOS within each band should be constant in space as indicated by Eq.(7) even in the disordered system. As the band-edge states preempt the DOS in the cells with low dielectric constant columns, there must be some states in this band concentrating in the cells with high dielectric constant columns. The C-numbers for the long-wave length region are distributed around zero, which is in accordance with the fact that the field is distributed uniformly in the system. When the degree of disorder is small($W = 0.1$), as shown in Fig. 19, this region of positive C in Fig. 19 (a) and (b) is not as obvious as in Fig. 18 (c) and (d), respectively. This implies that for weak disorder the band edge states do not occupy as much of the local DOS at the cells of low dielectric constant columns. This observation corroborates that the states at band edge for slightly disordered system are not as strongly localized as those for intermediate disordered system. Figure 20 shows there is no substantial increase of C-numbers in the positive region of the original lower band for the degree of disorder as high as $W = 1.2$. As we have seen in Fig. 16, when W is about 0.6 for

the TM mode and 0.4 for the TE mode, the localization due to the Bragg scattering begins to fade away, whereas this kind of localization was growing stronger consistently for lower values of W. One distinct feature of this Bragg-type of localization is the strong localization of states at the band edge and, as revealed here, the accompanying positive C-number region at certain lower frequency range, which implies the localization of the states around the cells with high dielectric constants in this lower frequency range.

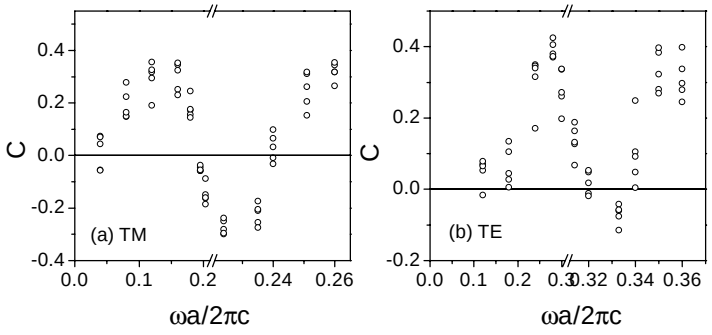

Fig. 20

The picture is now clear. The localization center distribution is established in the weak disorder range by long-range coherence. However, in the strong disorder range, this distribution is modified, or destroyed particularly in some frequency ranges(near original gaps). When the disorder is very strong, the localization centers separated in space are no longer connected by long-range coherence, therefore these centers do not necessarily have similar dielectric constants. In fact, for strong disorder, depending on the surrounding cells, a cell with a column of a high dielectric constant may have the same local energy level as the one with a low dielectric constant. As the disorder increases, the possibility increases of two disparate centers with the same local energy level arising within the localization length of each other. Then some states having disparate localization centers may be present. This is the microscopic interpretation of the presence of neutral C-numbers in the original gap.

E. Conclusion

We numerically studied the localization of light in the disordered dielectric structures derived from periodic systems with PBG. It was directly shown by field pattern that there existed strongly localized states in the original gap. The three-stage localization-delocalization process verifies the "interplay between the order and disorder" that has been suggested for a long time. We further point out that the trilogy arises because of different ranges of coherence for two kinds of localization mechanisms. Due to their different sensitivities to the two localization mechanisms, the TM and TE modes exhibit different localization behaviors. A new measure, the C-number was introduced to gain a deeper insight into the nature of localization. It was found with this number that the localization centers are not random, but that states prefer to localize at a specific kind of cells in a specific frequency range. In Anderson Model, there is only one band. The interaction of adjacent bands is neglected in the model. However, our results show that this kind of interaction may completely change the picture of localization. Most of our new results shown in this chapter of the report is due to the interaction of the adjacent bands. We propose the presence of states with neutral C numbers or the violation of the sum rule given in section C of this chapter may be regarded as a criteria of the case where Anderson model is not applicable.

VI. ACKNOWLEDGEMENTS

I must first thank Dr. Herbert Berk for his support and advice. Without his dedication and continuous encouragement, this thesis would not have been successful. I would also like to thank Dr. Qian Niu for his advice and dedication.

These two years in U. S., with the accomplishment of this thesis, I had a lot of experience in study and life. Some events were really excruciating. Thanks to my friends, I got over them. In particular, I would thank Yalin Xiong, whose unconstrained character saved me from the restraint of stereotype. Thanks to Chew- here Wang, who made me happy. I would also thank Dingyuan Lu and Idiom Yu Chen, who shared my happiness and sadness during these two years. Thanks to my previous supervisor Prof. C. D. Gong in China, who always gave me encouragement and support. Thanks to my friends Yin Lu and Zhou Wang, who are though not experts in expressing their affections, but experts in helping me in reality. Thanks to Weijang Yu, my previous roommate, whose computer helped me finished my first paper published on Physical Review B.

I would like to thank the genial faculty and staff at the University of Texas at Austin. I should not forget to thank Cherie Grandy, the manager of Terra Vista Apartments, whose friendliness facilitated my life. Thanks to Dr. Shanhui Fan for permission of using some of the figures.

Finally, I am grateful to my parents who always urge me to pursuing higher objectives. Thanks to my uncle Jiayuan Jiang, aunt Julie Jiang, Jufang Jiang, whose support is important to me.

APPENDIX A: CALCULATION OF THE REDUCED GREEN FUNCTION IN THE SUBSPACE OF THE LOCALIZED STATES

When there is no direction interaction between the propagating states, the Green function in the subspace of the localized states, or equivalently, the self-energy in this subspace completely determines the scattering process of the system.

The Green function is given by

$$G = G^0 \sum_{n=0}^{\infty} (VG^0)^n. \tag{A1}$$

where G^0 is the unperturbed Green function, being either G_c or G_k (the unperturbed Green function of the localized states and propagating states, respectively), and V can be V_{ck} or V_{c_1,c_2}. From now on, we consider only the matrix elements of G in the l-dimensional subspace of the localized states. Therefore, the initial and final states are both localized states. This means V_{ck} (or its hermitian conjugate) must be present for even times in each item of the summation. Because there is no direct interaction between propagating states, one such interaction must be followed by another, which returns the photon back to a localized states. Therefore, one can regard the following product as a whole in each item of the summation

$$V_{c_2,k} G^0_{kk} V_{k,c_1} \tag{A2}$$

note this product is an element of a matrix U of dimension $l \times l$, i.e. U represents an effective interaction in the subspace due to the indirection coupling of localized states through the propagating states. Now one easily shows that the G can written as

$$G = G^0 \sum_{m,n} \sum_{P} P\left(A^m B^n\right) \tag{A3}$$

where the summation of m and n run through all non-negative integers, the summation of P runs over any non-identical sequence(or permutation) of the product composed of m matrix A and n matrix B, and $A = UG^0$ and $B = VG^0$, in which G^0, U and V are restricted to the subspace of localized states.

This sum can be viewed in another way. Let us fix n and consider the summation of m and P first. It is not difficult to see that between any two B's in a sum item having n matrice B, the matrix A can appears arbitrary number of times, starting from zero. And each of these presence gives an independent contribution with weight 1. This means between any two B's (and before the first B and after the last B), there will be an infinite sum of arbitrary powers of A, which is just $(1-A)^{-1}$. Now the sum is easily performed over m

$$\begin{aligned} G &= G^0 \sum_n \left((1-A)^{-1}B\right)^n (1-A)^{-1} \\ &= G^0 \left[1-(1-A)^{-1}B\right]^{-1} (1-A)^{-1} \\ &= G^0 \left(1-UG^0-VG^0\right)^{-1} \\ &= \left(1-G^0U-G^0V\right)^{-1} G^0 \end{aligned} \tag{A4}$$

Obviously, the self-energy is just $\Sigma = U+V$ or in elements

$$\Sigma_{c_1,c_2} = V_{c_1,c_2} + \frac{1}{L}\sum_q V_{c_1,q} \frac{1}{\omega-\omega_q+i\epsilon} V_{q,c_2} \tag{A5}$$

REFERENCES

[1] J. D. Joannopoulos, P. R. Villeneuve, and S. Fan, Nature **386**, 143 (1997).

[2] S. John, Phys. Rev. Lett. **53**, 2169 (1984).

[3] E. Yablonovitch, Phys. Rev. Lett. **58**, 2059 (1987).

[4] A. Mekis, J. C. Chen, I. Kurland, S. Fan, P. R. Villeneuve, and J. D. Joannopoulos, Phys. Rev. Lett. **77**, 3787 (1996).

[5] S.-Y. Lin, E. Chow, V. Hietala, P. R. Villeneuve, and J. D. Joannopoulos, Science **282**, 274 (1998).

[6] E. A. J. Marcatili, Bell Syst. Tech. J., 2071 (1969); E. A. J. Marcatili, *ibid.* 2103 (1969).

[7] S. Fan, P. R. Villeneuve, and J. D. Joannopoulos, Phys. Rev. Lett. **80**, 960 (1998).

[8] S. Fan, P. R. Villeneuve, J. D. Joannopoulos, M. J. Khan, C. Manolatou, and H. A. Haus, Phys. Rev. B, **59**, 15882 (1999).

[9] P. W. Anderson, Phys. Rev. **109**, 1492 (1958).

[10] N. F. Mott, Adv. Phys. **16**, 49 (1967), and Philos, Mag. **17**, 1259 (1968).

[11] say, E. Abraham, P. W. Anderson, D. C. Licciardello, and T. V. Ramakrishnan, Phys. Rev. Lett. **42**, 673 (1979).

[12] P. W. Anderson, Philos. Mag. B **52**, 505 (1985); K. Arya, Z. B. Su, and J. L. Birman, Phys. Rev. Lett. **57**, 1879 (1986); C. A. Condat and T. R. Kirkpatrick, Phys. Rev. Lett. **58**, 226 (1987).

[13] Y. Kuga, and A. Ishimaru, J. Opt. Soc. Am. A **1**, 831 (1984); M. P. van Albada and A. Lagendijk, Phys. Rev. Lett. **55**, 2692 (1985); P. R. Wolf and G. Maret, Phys. Rev. Lett. **55**, 2696 (1985); S. Etemad, R. Thomson, and M. J. Andrejco. Phys. Rev. Lett. **57**, 575 (1986).

[14] S. John, Phys. Today **44**, 32 (1991).

[15] S. John, Phys. Rev. Lett. **58**, 2468 (1987).

[16] Q. Jiang and R.-B. Tao, Phys. Rev. B **43**, 6136(1991).

[17] M. M. Sigalas, C. M. Soukoulis, C.-T. Chan, and D. Turner, Phys. Rev. B **53**, 8340 (1996).

[18] V. D. Freilikher, B. A. Liansky, I. V. Yurkevich, A. A. Maradudin, A. R. McGurn, Phys. Rev. E **51**, 6301 (1995).

[19] M. Drake, A. Z. Genack, Phys. Rev, Lett. **63**, 259 (1989).

[20] Hans De Raedt, Ad Lagendijk, and Pedro de Vries, Phys. Rev. Lett. **62**, 47 (1989); A.R. Mcgurn and P. Sheng and A. A. Maradudin, Optics Commun. **91**, 175 (1992).

[21] W. Jiang and C. D. Gong, Phys. Rev. B **60** 12015 (1999).

[22] E. Ozbay and B. Temelkuran, Appl. Phys. Lett. **69**, 743 (1996).

[23] B. Temelkuran and E. Ozbay, Appl. Phys. Lett. **74**, 486 (1999).

[24] P. Yeh, *Optical Waves in Layered Media* (John Wiley & Sons, New York, 1988).

[25] For a recent review, see M. S. Kushwaha, Intern. J. Mod. Phys. B, **10**, 977 (1996).

[26] E. R. Brown, C. D. Parker and E. Yablonovitch, J. Opt. Soc. Am. B **10**, 440 (1993).

[27] J. S. Langer and T. Neal, Phys. Rev. Lett. **16**, 984 (1966).

[28] R. D. Meade, K. D. Brommer, A. M. Rappe, J. D. Joannopoulos, and O. L. Alerhand, Phys. Rev. B **48**, 8434 (1993). For a detailed treatment of the algorithm, refer to M. P. Teter *et. al.* Phys. Rev. B **40**, 12,255 (1989).

[29] P. Dean, Proc. Phys. Soc. (London) **73**, 413 (1959); P. Dean, Proc. Roy. Soc. (London) A **254** 507 (1960).

[30] For example, X.-P. Feng and Y. Arakawa, Jpn. J. App. Phys. **36**, L120 (1997).

[31] For the numerical calculations of Anderson model and some generalized cases, see F. Yonezawa, J. Non-Cryst. Solids **35** & **36**, 29 (1980).

[32] A. F. Ioffe and A. R. Regel, Prog. Semicond. **4**, 237 (1960).

[33] J. D. Joannopoulos, R. D. Meade, and J. N. Winn, *Photonic Cyrstals: molding the flow of light* (Princeton University Press, Princeton, 1995).